Influence of Molecular Polarizability on the Active Layer of Organic Photovoltaic Cells: A case study of Poly(3-hexylthiophene)

By

Cornah, Bennie Elizabeth

A Thesis
Submitted to the African University of Science and Technology
Abuja-Nigeria

In Partial Fulfillment of the Requirements for the
Award of Master of Science Degree in Theoretical Physics

Supervisor: **Dr. Omololu AKIN-OJO**

MAY, 2013

Influence of Molecular Polarizability on the Active Layer of Organic Photovoltaic Cells: A case study of Poly(3-hexylthiophene)

A THESIS APPROVED

BY

SUPERVISOR.....
Dr. Omololu AKIN-OJO

MEMBER.....

Dedication

I wish to dedicate this work to my dearest and beloved father for his endless love, support and sacrifices in seeing me through my education.

Also, my dedication goes to my siblings, Morkeh, Rosina, Philomena and Linda, not forgetting my beloved friend Benjamen for their encouragement and support during my stay at the African University of Science and Technology (AUST).

Acknowledgement

First and foremost, I wish to thank the Almighty God for bringing me this far, endowing me with wisdom, knowledge and understanding over these years.

I wish to express my sincere gratitude to my supervisor, Dr. Omololu AKIN-OJO for his support, guidance, assistance and time in supervising my work. His great efforts to explain things in a clear and simple way have greatly influenced my way of thinking and approach to scientific research.

I would also like to thank all the visiting faculties of the Department Theoretical Physics (African University of Science and Technology) for the rich knowledge and skills they imparted to me during my M.Sc. in Theoretical Physics program.

My appreciation goes to the CHPC group in South Africa and ICTP in Italy for granting me the opportunity to use their computer system for my simulation. without whom it would have been impossible to get any results at all. Thank you for your generosity.
To Usman, I say thanks very much for your care, support, encouragement and advices, you are indeed a wonderful friend.
To Benjamen, I say thanks for everything.

Last but not the least, I would like to give my heartfelt thanks to my father.

Abstract

The complexity of the microstructure of the active layer in organic photovoltaics (OPVs) poses a unique challenge in improving the efficiency of OPV devices. Molecular dynamics (MD) simulation provides a direct route to determining this microstructure. However, for a donor material like poly (3-hexylthiophene), $(P3HT)_n$, approximations made in all previous force field for MD simulation has been the neglect of explicit polarization. We looked at the morphology of $(P3HT)_n$ using MD simulations at different temperatures where we confirmed the semi-crystalline behavior of P3HT between temperatures of 300 K and 400 K. In line with this, we developed force fields from *ab initio* data with and without inclusion of explicit molecular polarizability for dimers of $(P3HT)_1$ with monomers optimized at the MP2/cc-pvtz level.

Contents

Dedication ii

Acknowledgement iii

Abstract iv

Nomenclature ix

1 Introduction 2

2 Atomistic Structure and Dynamics of Poly(3 hexyl-thiophene) 8
- 2.1 Structure and Properties of P3HT . . . 8
  - 2.1.1 Regioregularity in P3HT . . . 9
- 2.2 Molecular Interactions . . . 11
  - 2.2.1 Short Range Repulsive Interaction . . . 11
  - 2.2.2 Dipole Interaction . . . 12
  - 2.2.3 Polarization . . . 13
  - 2.2.4 Dipole Polarizability . . . 15
  - 2.2.5 Static Dipole Polarizability . . . 15

3 Computer Simulation 19
- 3.1 Theoretical Models . . . 20
- 3.2 Basis sets . . . 22
  - 3.2.1 Types of Basis Set . . . 23
- 3.3 Geometry Optimization . . . 25
- 3.4 Force Fields . . . 26
  - 3.4.1 Force Field Development . . . 27

4 MD Simulation of Poly(3-hexylthiophene) 31
- 4.1 Development of P3HT Molecular Structure and Geometry Optimization . . . 31
- 4.2 Molecular Dynamics Simulation . . . 34

4.3 Results and Discussions 36
4.4 Development of Ab Initio Polarizable Force Fields for $(P3HT)_1$ 38
4.4.1 *Ab Initio* Atomic Partial Charges 45
4.4.2 *Ab Initio* Distributed Polarizabilities 47
4.4.3 *Ab Initio* Lennard Jones parameters 47

5 Conclusions and Recommendations **51**
5.1 Conclusion 51
5.2 Recommendation 51

Appendix **52**

List of Figures

1.1 IPV and OPV difference 2
1.2 Elecronic and Optical process in OPV 3
1.3 Hole mobility variation with Molecular weight 5

2.1 Chemical structure of P3HT 9
2.2 Chemical structure of RR-P3HT 10
2.3 Chemical structure of RRa-P3HT 10
2.4 Electro-negativity in water molecule 12
2.5 Induced dipole 13
2.6 Polarization in a neutral molecule 15

3.1 Curve for Slater and Gaussian type functions 23

4.1 Developed molecular structures 32
4.2 Starting geometry 35
4.3 Chemical structure of P3HT monomer 36
4.4 Molecular polarizability plots for $(P3HT)_n$ (n="0",1,2,3) . . . 38
4.5 RDF(C1–C1)at different temperature 39
4.6 RDF (C2–C2) at different temperature 40
4.7 RDF (C3–C3) at different temperature 41
4.8 RDF (C4–C4) at different temperature 42
4.9 RDF (C5–C5)at different temperature 43
4.10 RDF (S–S) at different temperature 44

List of Tables

4.1 *Final Configuration of Single Unit P3HT at MP2/6-311++G** level.* 33
4.2 *Computed polarizability values of various RR-P3HT units (i.e., n = 0, 1, 2, 3) at B3LYP/6-311G** level and the corresponding calculated isotropic polarizabilities (α_{iso}).* 34
4.3 *Non-bonded parameters (OPLS-AA model) used in atomistic simulation models of* $(P3HT)_1$. 37
4.4 *Optimized geometry of* $(P3HT)_1$ *with MP2/cc-pvtz* 45
4.5 *Ab initio* Partial Charges 46
4.6 *Ab Initio* Distributed Polarizability 48
4.7 *Ab Initio* Lennard-Jones Interaction Parameters 48

Nomenclature

P3HT	Poly (3-hexylthiophene)
PV	Photovoltaic
OPV	Organic photovoltaic
IPV	Inorganic photovoltaic
PCE	Power conversion efficiency
OSCs	Organic solar cells
MEH-PPV	Poly[2-methoxy-5-(2-ethylhexyloxy)-p-phenylenevinylene]
MDMO-PPV	Poly[2-methoxy-5-(3',7'-dimethyloctyloxy)-1,4-phenylenevinylene]
Zn Pc	Zinc phthalocyanine
RR	Regioregular
Ra	Regiorandom
MD	Molecular Dynamics
MW	Molecular weight
OPLS	Optimized potential for liquid simulation
OPLS-AA	Optimized potential for liquid simulation - all atom
n	Number of monomer chains or units
MC	Monte Carlo
DFT	Density functional theory
MM	Molecular mechanics
MPN	Moller-Plesset perturbation theory
CI	Configuration interaction
HF	Hartree- Fock
ZINDO	Zerner's Intermediate Neglect of Differential Overlap
AM1	Austin Model
MMFF	Molecular mechanics force field
UFF	Universal force field
B3LYP	Becke, 3-parameter Lee-Yang-Parr
S(v)	Slater function
G(v)	Gaussian function
STOs	Slater-type orbitals
GTOs	Gaussian-type orbitals

LCAO	Linear Combination of atomic orbitals
RDF	Radial distribution function
LJ	Lennard-Jones

Chapter 1

Introduction

As the world is faced with the issues of ever-decreasing fossil fuel and ever-increasing environmental crises resulting from greenhouse gas production, photovoltaic (PV) technology has become a main focus of attention. The success of any PV technology depends on its efficiency, lifetime and cost. Silicon-based solar cells (a type of IPV) have high efficiencies. However, the high cost to efficiency ratio of silicon-based solar cells and their complex production process has generated interest in developing alternative PV cells such as organic photovoltaics (OPVs). The obvious difference between IPVs and OPVs in terms of their photo-conversion mechanisms (Fig. 1.1) is that light absorption in OPV cells leads to the production of exciton mobile excited states while in IPVs, it leads directly to the creation of free electron-hole pairs.

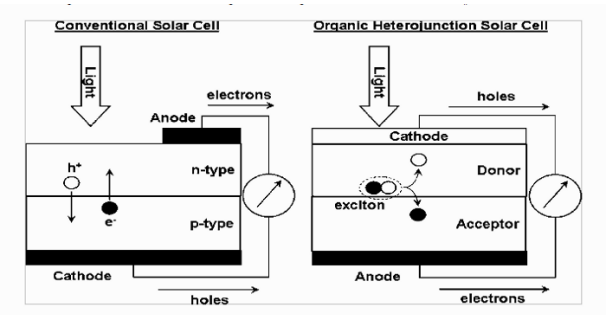

Figure 1.1: *Illustration on the difference between organic and inorganic solar cells when considering the photo-conversion process.*

Despite the fact that OPVs have lower efficiencies, developing high performance organic photovoltaic devices as sources of sustainable energy has been an important issue in research conducted worldwide in recent years due

to the low manufacturing cost of the devices and their use in the fabrication of flexible devices. In the last decade, the performance of OPVs has improved steadily, reaching a power conversion efficiency (PCE) as high as 7% [1]. It is the first PV technology capable of generating electricity at a cost on par with conventional fuels, making it a cost-effective renewable energy source without government subsidies. Although, there are other possible applications, the most common and promising application of OPV technology are in organic solar cells (OSCs).

In spite of the tremendous advancement in the power conversion efficiency of organic solar cells over the past decade, major efforts are still needed to understand and optimize all electronic and optical processes (Fig. 1.2) taking place in OPV devices to ensure a continuous increase of their performance. Figure 1.2 depicts how an OPV device operates the conversion of the incident solar irradiation to electrical current which involves processes such as photon absorption, exciton diffusion, charge separation and collection of charges.

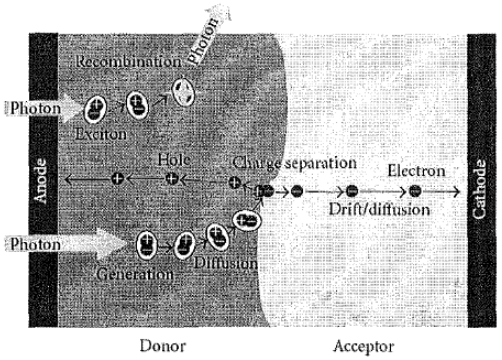

Figure 1.2: *Illustration of Elecronic and Optical process in OPV.*

One of the major causes of the low efficiency of OPVs has been the difficulty in improving the morphology of the active layer. Recent studies indicate that the efficiency of organic solar cells is highly correlated to the morphology of the interface between the donor and acceptor materials of the active layer (Fig. 1.2), which in turn depends on the preparation conditions, the crystallization of the particular materials, and the interaction between its donor and acceptor molecules. The problems in designing a high efficiency OPV are complicated by the fact that the texture, or morphology of the donor acceptor blend (which is sensitive to the exact conditions of how the blend was processed into a thin film) has a dramatic effect on the performance of the OPV [2]. In addition, photo-generation factors such as the exciton diffusion length, charge separation and charge collection which affect the performance are greatly influenced by the material morphology. For example exciton dif-

fusion length has been estimated to range between 10 – 100 nm. This implies that, the active layer interface should have as large an area as possible, and the morphology of the donor and acceptor materials (mostly conjugated polymers and Fullerene derivatives respectively) should be such that the charge carriers have unrestricted conduction pathways to their respective electrodes as suggested by Benanti and Venkataraman (2006). This brings to mind the concept of bulk heterojunction as introduced by Tang in 1986 [8]. By using bulk heterojunction as an alternative active layer structure, Tang recognized that the interface between the donor and acceptor materials, not the electrode contacts is the key to determining the photovoltaic properties of an OPV [3]. In a nutshell, to account for these characteristic properties, the interface morphology of OPV has to be well controlled. This, makes the material morphology essential to improving the efficiency of OPVs.

The question then is, how do we improve the constituents of the active layer in OPVs and what measures need to be taken with regards to the donor or acceptor materials used in OPVs in order to give the charge carriers unrestricted pathways to their respective electrode? These are the questions we wish to answer in this work with a focus on the poly 3-hexylthiophene (P3HT) donor material. P3HT exhibits lower band gap, broader spectra and also better hole mobility compared to other classic conjugated polymers such as poly[2-methoxy-5-(2-ethylhexyloxy)-p-phenylene vinylene] (MEH-PPV), MDMO-PPV, Zn Pc and even other polythiophenes that are broadly used as the donor material in OPV.

A lot of research work has been done both experimentally and theoretically in studying this material. For example, Kline *et. al.*, in their work, showed a clear correlation between the field-effect mobility of regioregular P3HT (RR-P3HT) and its molecular weight with mobility values increasing from 1.7×10^{-6} to 9.4×10^{-3} $cm^2 v^{-1} s^{-1}$ as the molecular weight is increased from 3.2 to 36.5 kD, where they suggested that optimizing the molecular weight (MW) of conjugated polymers could lead to significant improvements in the device performance [4]. Computationally, Nelson *et al.*, confirmed that via molecular dynamics (MD) simulations, coarse-grained models of the molecular packing can be used to rationalize the MW dependence of hole mobility in regioregular polythiophene (depicted by Fig. 1.3). It can be observed in figure 1.3 that the simulated hole mobility (filled stars) increases with increasing MW which is in agreement with the experimental observations(open triangles) [5].

Phase transition kinetics in P3HT has also been studied using differential scanning calorimetry (d.s.c.) where it was revealed that the phase transitions in P3HT are characterized by two separate, i.e. one fast and one slow, crystal

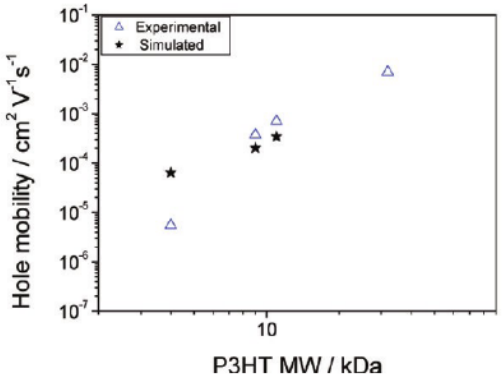

Figure 1.3: *Simulated low-field limit time-of-flight mobility (filled stars) in comparison with measured Field-Effect Transistors mobilities(open triangles).*

formation processes, which supports the existence of the ordered nematic state in the melt of P3HT [6].

Due to the complex nature of the active layer microstructure, experiments to determine the morphology on the nanoscale are difficult. Molecular dynamics (MD) simulations offer a direct route to determining these microstructures. MD simulations however depend on accurate force fields. Force fields determined from experiments are the most popular for simulations of P3HT. However, these force fields are not accurate. For example, Freisner and coworkers implemented adjustments to the (Optimized Potential for Liquid Simulation) OPLS-2005 force field in order to improve its ability to model systems such as P3HT where they show the impact of these changes on the dihedral angle distributions, persistence lengths, and conjugation length distributions observed during molecular dynamics simulations [7]. Despite the fact that P3HT has a huge molecular polarizability, one particular approximation in all previous force fields is the neglect of explicit polarization.
In this work, we plan to examine the influence of the molecular polarizability of P3HT on its morphology at different temperatures and to develop a polarizable force field based on ab initio data.

Organization of Thesis Work

This thesis is organized as follows:

- **Chapter Two**: The properties, structure of P3HT monomer chains (denoted $(P3HT)_n$) are studied. Polarizability in molecules is also

described.

- **Chapter Three**: An overview of computer simulation is given.
- **Chapter Four**: MD simulations of $(P3HT)_n$ (n="0", 1, 2 and 3) and development of a polarizable *ab initio* force field are described.
- **Chapter Five**: Conclusions and suggestions for future studies are given.

Bibliography

[1] Xiangjian Wan, Guankui Long, Lu Huang, and Yongsheng Chen, Graphene A Promising Material for Organic Photovoltaic Cells *Adv. Mater.*, 2011, 23, 53425358.

[2] A. Opitz, J. Wagner, W. Brutting, Ingo Salzmann, N. Koch, J. Manara, J. Pflaum, A. Hinderhofer, and Frank Schreiber, "Interfaces: Correlation Between Morphology and Solar Cell Performance", *IEEE Journal of Selected Topics in Quantum Electronics*, Vol. 16, No. 6, 2010.

[3] Travis L. Benanti and D. Venkataraman, Organic solar cells: An overview focusing on active layer morphology *Photosynthesis Research*, 87: 7381, 2006.

[4] Chiatzun Goh, R. Joseph Kline, Michael D. McGehee, Ekaterina N. Kadnikova and Jean M. J. Frchet, "Molecular-weight-dependent mobilities in regioregular poly(3-hexyl-thiophene) diodes", *Appl. Phys. Lett.* **86** 122110, 2005.

[5] Jenny Nelson, Joe J. Kwiatkowski, James Kirkpatrick and Jarvist M. Frost, "Modeling Charge Transport in Organic Photovoltaic Materials", Department of Physics, Imperial College London, Blackett Laboratory, Prince Consort Road, London SW7 2AZ, United Kingdom, 2009.

[6] Yue Zhao, Guoxiong Yuan, Mario Leclerc and Philippe Roche, "A calorimetric study of the phase transitions in poly(3-hexylthiophene)", *Polymer Vol.* 36 No. 11, pp. 2211-2214, 1995.

[7] Kateri H. DuBay, Michelle Lynn Hall, Chuanjie Wu, David R. Reichman, and Richard A. Friesner, "Accurate Force Field Development for Modeling Conjugated Polymers", *Journal of Chemical Theory and Computation.*

[8] C. W. Tang, "Two-layer organic photovoltaic cell", *Appl. Phys. Lett.* **48** 183, 1986.

Chapter 2

Atomistic Structure and Dynamics of Poly(3 hexyl-thiophene)

In this chapter, the properties and structure of $(P3HT)_n$ are discussed. We also give an overview of molecular interactions, dipole moments and polarizabilities in molecules.

2.1 Structure and Properties of P3HT

P3HT, poly(3-hexylthiophene) (Fig. 2.1) belongs to the class of conjugated polymers. It comprises of three atoms namely carbon (C), hydrogen (H) and sulfur (S). A single unit of P3HT can be divided into two parts, the thiophene part and the alkyl part (i.e., C_nH_{2n+1} where n = 6).

It is one of the most studied poly(3-alkylthiophene)s used as a donor in OPV devices. Basically, the crystal of P3HT is formed by aligned chains which are stacked on top of each other, with the thiophene rings forming a planar alternating 'up-down' conformation and the alkyl side chains pointing perpendicularly to the stacking direction. Despite the many studies performed and reported in literature, the actual structure of P3HT in the solid state seems to be complicated and continues to be the subject of further investigations. An interesting feature of P3HT is a possible liquid crystalline state after the crystal melting. It has also been revealed that the phase transitions in P3HT are characterized by two separate (i.e., one fast and one slow) crystal formation processes, which supports the existence of the ordered nematic state in the melt of P3HT [1].

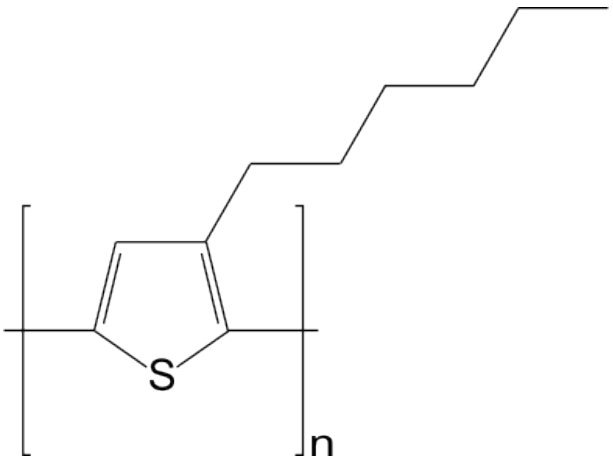

Figure 2.1: *Chemical structure of poly(3-hexylthiophene) (P3HT). Where n represents the number of P3HT molecular units.*

In OPV, P3HT is the most commonly used donor material in the active layer of OPV cells because of :

- its lower band gap (1.9 eV) compared to PPV which has a band gap higher than 2.0 eV
- its higher absorption coefficient (close to the maximum photon flux in the solar spectrum).
- it being known as a high-mobility material in the field of organic electronics.

Despite the achievements that have been made towards improving the mobility of conjugated polymers such as P3HT, much is still not known about how charges move through the films and how the chain packing can be optimized to obtain even higher mobilities. This is one of the motivations for this thesis work, to device a computational means to optimize the chain packing and the P3HT molecule as a whole via MD simulations in order to predict its condensed phase structure.

2.1.1 Regioregularity in P3HT

The term *regioregularity* (denoted by either rr or RR) is used to describe a polymer in which each repeat unit is derived from the same isomer of the monomer. Regioregularity of conjugated polymers is an important factor in determining their higher order structures in solid state and molecular orientation. Crystalline packing of the regioregular polymers provides intra-

and inter-molecular ordering of the conjugating polymer chains in the films. This leads to enhanced light absorption and higher charge mobilities that is desirable for various optoelectronic device applications such as organic field effect transistors and photovoltaic devices.

P3HT exhibits three different regioregularities (Figures 2.2 and 2.3) namely: (a) regiorandom (or regio-irregular), (b) regioregular with medium regioregularity (with $RR \sim 94\%$) and (c) regioregular with very high regioregularity (with $RR \sim 98\%$). (b) and (c) show typical absorption features of ordered lamellar structure of P3HT in the solid state even without annealing while films of regiorandom P3HT, (a) are very disordered as indicated by their broad and featureless absorption.

This structural difference in the solid state coincides with partially non-dispersive transport and hole mobilities, μ_h of around 10^{-4} and $10^{-5} cm^2 v^{-1} s^{-1}$ for high and medium regioregular P3HT, respectively, and a slow and dispersive charge transport for regiorandom P3HT [2]. Among the materials

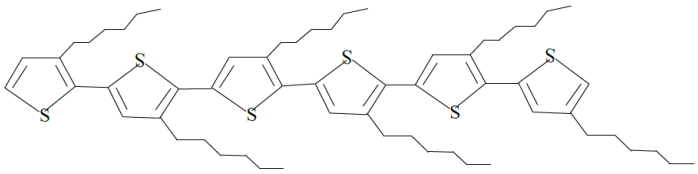

Figure 2.2: *Chemical structure of regioregular Poly-(3-hexylthiophene), (RRP3HT with n=6).*

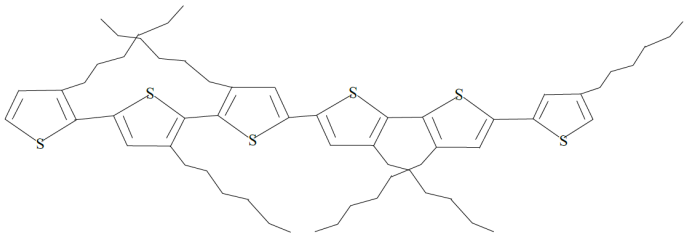

Figure 2.3: *Chemical structure of regiorandom Poly(3-hexylthiophene), (Ra-P3HT with n=6).*

for OPV investigated so far, regioregular poly(3-hexylthiophene) (RR-P3HT Fig. 2.2) has demonstrated promising physical properties, such as environmental stability, reasonably high hole mobility, and an improved absorption as compared with PPV-based devices. It should be noted that RR-P3HT

self-organizes into a crystalline structure and, owing to the pp stacking direction, the charge (hole) transport is extremely efficient. The properties of RR-P3HT mentioned above make P3HT a very useful and important material for improving charge transport in the active layer of OPVs . This also explains why a lot of research is being done in recent times to investigate P3HT polymer.

In organic molecules such as P3HT, dipole polarizabilities are important parameters. This is due to the fact that dielectric constants, optical rotatory dispersion, other optical properties and Raman scattering are manifestations of the capability of a substance to be polarized by an electric field. Many properties can be predicted by accounting for charge polarization. So, the capabilities to accurately predict or model polarizabilities are of immediate utility in the evaluation of certain macroscopic properties as well as in analysis of weak interactions [4]. The primary electronic structure change that occurs in weakly interacting closed-shell species is that attributable to charge polarization. In the next section, a fundamental understanding of molecular interaction in relation to polarization is elaborated where a formular for molecular static dipole polarizability is derived.

2.2 Molecular Interactions

All molecular interactions are fundamentally electrostatic in nature and can be described by Coulombs Law. Coulomb's law correctly describes forces that bind; (1) electrons to nuclei in atoms, (2) atoms to atoms in molecules, and (3) molecules to molecules in liquids and solids. There are many different ways of parsing molecular interactions. For our purpose only two will be discussed. These are Short range repulsive interaction and Dipole interaction.

2.2.1 Short Range Repulsive Interaction

When two non-bonded atoms approach each other at a distance, overlap of the occupied orbitals results in electrostatic repulsion between the electrons of those atoms. This repulsive energy acts over a very short range, but goes up very sharply when that range is violated. The repulsion goes up as $1/R^{12}$ where R is the distance between two non-bonded atoms. This is important only when atoms are in very close proximity. Because this repulsive term rises so sharply as distance decreases, it is sometimes reasonable to think of atoms as hard spheres, like small pool balls, defined by Van der Waals radii and surfaces. In addition, When two atoms approach each other their Van

der Waals surfaces make contact when the distance between them reaches the sum of their Van der Waals radii. Here, it is assumed that bonds do not form. When bonds form, Van der Waals radii are violated. The smallest distance between two non-bonded atoms is the sum of the van der Waals radii of the two atoms.

2.2.2 Dipole Interaction

In a molecule with unlike atoms, electrons are not shared equally. The tendency of any atom to pull electrons away from other atoms is characterized by a quantity called electro-negativity. Thus when a molecule is composed of atoms of various electro-negativities, the atoms with lowest electro-negativities hold partial positive charges and the atoms with the greatest electro-negativities hold partial negative charges (this is illustrated in the picture (Fig. 2.4) for water molecule below). The extent of charge separa-

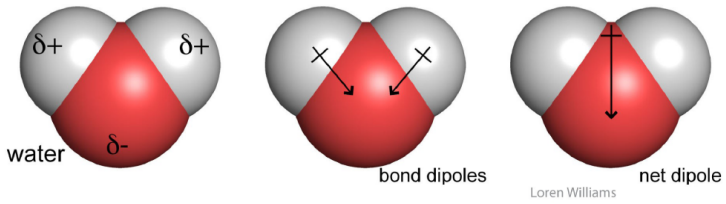

Figure 2.4: *This picture depicts how in water molecule, the electro-negative oxygen atom pulls electron density away from the hydrogen atoms thereby making water polar. The oxygen atom carries a partial negative charge and the hydrogen atoms carry a partial positive charge.*

tion within a molecule is characterized by the dipole moment (μ), which is mostly measured in Debye units.

A dipole can interact with point charges (called Charge-Dipole Interaction), other dipoles (called Dipole-Dipole Interaction), and can induce charge distribution in surrounding molecules (called Dipole-Induced Dipole Interaction). For the Charge-Dipole Interaction, a molecule with a permanent dipole can interact favorably with charged species. This type of interaction is why sodium chloride (charged) interacts well with water (dipole). With Dipole-Dipole Interaction, the interaction energy between two dipoles can be either positive or negative and can be calculated with Coulomb's Law; however, the interaction fall off with $1/r^3$. For Dipole-Induced Dipole Interaction, a molecule with a permanent dipole can induce a dipole in a second molecule that is located nearby in space. The strength of the interaction depends

on the dipole moment of the first molecule and the polarizability of the second. Molecules with π-electrons, such as benzene and phenylalanine are more polarizable than molecules without π-electrons. Dipole-Induced Dipole Interactions are always attractive and can contribute as much as 0.5 kcal/mole to stabilization but this interaction falls off as $1/r^4$ [3].

2.2.3 Polarization

Polarization is important for two reasons:

- Inter-molecular polarization is necessary to describe gas-phase and condensed-phase properties within a single model.
- Intra-molecular polarization is needed to treat the conformational dependence of electrostatics.

Neutral non-polar species have spherically symmetric arrangements of electrons in their electron clouds and as a result when in the presence of an electric field, their electron clouds can be distorted. The ease of this distortion is defined as the *polarizability* of the atom or molecule which causes the originally non-polar molecule or atom to acquire a dipole moment. This induced dipole moment, μ_{ind} is related to the polarizability of the molecule (or atom) and the strength of the electric field by the following equation:

$$\mu_{ind} = \alpha E \tag{2.1}$$

Where, α is the constant of proportionality called *atomic polarizability* and E denotes the strength of the electric field. μ_{ind} is linear provided E is not too big. If we imagine a one-electron atom with a radius of R placed in an external electric field (Fig. 2.5), the electrons orbit will be shifted away from the nucleus by a distance, d. Then the induced dipole is given by:

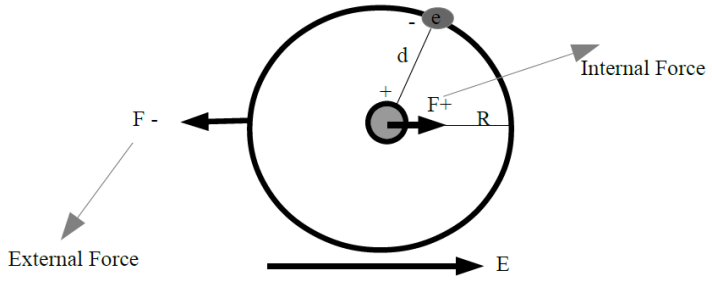

Figure 2.5: *One-electron atom in an external electric field.*

$$\mu_{ind} = \alpha E = de \tag{2.2}$$

At the equilibrium value of d, the external force, F_{ext} on the electron due to the field must exactly counterbalance the internal force, F_{int} of displacement between the nucleus and the electron. In other words, the equilibrium position of the nucleus is that position where the external force is canceled by the force exerted on it by the electron cloud, that is:

$$F_{ext} = F_{int} \tag{2.3}$$

where these forces are given by the expressions:

$$F_{ext} = eE \tag{2.4}$$

$$F_{int} = eE(d) = \frac{e^2 d}{4\pi\varepsilon_0 R^3} \tag{2.5}$$

Where ε_0 is the electric permittivity of free space. Substituting Equations 2.4 and 2.5 into 2.3, the equilibrium displacement, d between the nucleus and the electron, can be expressed as:

$$d = \frac{4\pi\varepsilon_0 R^3 E}{e} \tag{2.6}$$

Which implies that d is linearly proportional to the external electric field, E. Therefore, substituting Eq. 2.6 into 2.2, we can rewrite equation 2.2 as:

$$\mu_{ind} = \alpha E = 4\pi\varepsilon_0 R^3 E \tag{2.7}$$

From which, the polarizability can be expressed as:

$$\alpha = \frac{\mu_{ind}}{E} = 4\pi\varepsilon_0 R^3 \tag{2.8}$$

Neglecting the permittivity term (ε_0), the polarizability should be roughly equal to the volume of the atom.

Although this model of the atom is extremely crude, it produces results that are in reasonable agreement with direct measurements of the atomic polarizability. The best approach follows from Quantum Mechanics as shown in the next section.

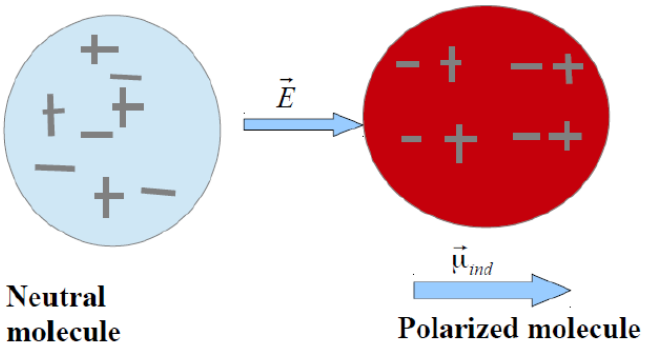

Figure 2.6: *Illustration of polarization in a neutral molecule.*

2.2.4 Dipole Polarizability

Polarizability characterizes how readily the atomic or molecular charge distribution is distorted by external static or oscillating electromagnetic fields. Consequently, it depends on the electronic structure of atoms and molecules. When an atom or molecule interacts with an external electric field, the atom (or molecule) is polarized and the resulting charge distribution is characterized by induced electric multipole moments. Of these multipole moments, the induced dipole moment (μ_{ind}) is related to the electric field (E) through the dipole polarizability (Fig. 2.6) where as, the quadrupole moment is related to the electric field gradient through the field-gradient polarizability.

Polarizability can either be static or dynamic (depends on oscillating electromagnetic field). In this thesis work however, static polarizability is studied. Static electric dipole polarizability of an atom or a molecule describes the changes in the charge distribution when it interacts with an external electric field. It is a linear response property and is defined as the second derivative of the total energy of the system with respect to an external homogeneous electric field. Several computer programs (such as Gaussian 09 and ORCA) can be used to calculate this molecular property (as used in this work).

2.2.5 Static Dipole Polarizability

The expression for static dipole polarizability follows from perturbation theory in quantum mechanics. The perturbation expression for the total energy, E for the ground state $|0\rangle$ is:

$$E = E_0^{(0)} + \langle 0|H^{(1)}|0\rangle + \sum_{n\neq 0} \frac{\langle 0|H^{(1)}|n\rangle\langle n|H^{(1)}|0\rangle}{E_0 - E_n} + \dots \tag{2.9}$$

where, $E_0^{(0)}$ is energy for the unperturbed system (or the zero point energy), the second and third terms on the right hand side of Eq. 2.9 are the first and second order corrections to the ground state energy respectively, with $H^{(1)}$ as the perturbation term.

A homogeneous electric field perturbation along the x-axis, $H^{(1)} = -\mu_x F$ gives:

$$E = E_0^{(0)} - \langle 0|\mu_x|0\rangle F + \left(\sum_{n\neq 0} \frac{\langle 0|\mu_x|n\rangle\langle n|\mu_x|0\rangle}{E_0 - E_n}\right) F^2 + \dots \tag{2.10}$$

The static dipole polarizability is defined as the second derivative of the above expression (Eq. 2.10) with respect to the field strength, F at $F = 0$ such that

$$\begin{aligned}\alpha_{xx} &= -\left(\frac{d^2E}{dF^2}\right)_{F=0} = \left(\frac{d}{dF}\langle 0|\mu_x|0\rangle\right)_0 - \left(\frac{d}{dF}\sum_{n\neq 0}\frac{\langle 0|\mu_x|n\rangle\langle n|\mu_x|0\rangle}{E_0 - E_n}F\right)_0 \\ &= 2\sum_{n\neq 0}\frac{\langle 0|\mu_x|n\rangle\langle n|\mu_x|0\rangle}{E_n - E_0}\end{aligned} \tag{2.11}$$

In the above expression, the first derivative results in the expectation value of the dipole moment operator, μ_x which gives the permanent electric dipole moment.
Equation 2.11 shows dipole polarizability, α_{xx} with two subscripts. This is because the dipole polarizability is regarded as a second rank tensor.
When an external field (F) is applied along the x-axis, a dipole may be induced with components μ_x, μ_y and μ_z where,

$$\mu_\beta = \sum_\gamma \alpha_{\beta\gamma} F_\gamma \quad \beta, \gamma = x, y, z \tag{2.12}$$

In general, the diagonal element, α_{xx} dominates the other two when the electric field is along the x-axis, as the induced dipole moment is usually almost parallel to the applied electric field. For example, in a closed-shell atom the dipole polarizability can be reduced to a scalar quantity in which the only surviving polarizability tensor component is the one parallel to the applied electric field.

If we denote the excitation energy, $E_n - E_0$ by ΔE_{n0} and the matrix element, $\langle 0|\mu_x|n\rangle$

by $\mu_{x,0n}$ not forgetting the fact that the dipole moment operator is a Hermitian operator so that $\langle 0|\mu_x|n\rangle = \langle n|\mu_x|0\rangle$. Then Eq. 2.11 is simplified to

$$\alpha_{xx} = 2\sum_{n\neq 0} \frac{\mu^2_{x,0n}}{\Delta E_{n0}} \tag{2.13}$$

Using the explicit expression in Eq. 2.11 for the static dipole polarizability, similar expressions can be written for polarizabilities with a field applied along the y- or z-axis, that is

$$\alpha_{yy} = 2\sum_{n\neq 0} \frac{\mu^2_{y,0n}}{\Delta E_{n0}} \tag{2.14}$$

$$\alpha_{zz} = 2\sum_{n\neq 0} \frac{\mu^2_{z,0n}}{\Delta E_{n0}} \tag{2.15}$$

Equations 2.12, 2.13 and 2.14 are the theoretical equations used for numerical calculation of polarizability in which case, the quantum chemistry program used computes values for polarizabilities with field applied parallel (along) and perpendicular to the x-, y-, and z-axis (i.e., includes values for α_{xy}, α_{xz}, α_{yx}, α_{yz} α_{zx}, α_{zy}). This implies that the polarizability tensor, α in general has nine components as shown in the 3×3 matrix below:

$$\alpha = \begin{bmatrix} \alpha_{xx} & \alpha_{xy} & \alpha_{xz} \\ \alpha_{yx} & \alpha_{yy} & \alpha_{yz} \\ \alpha_{zx} & \alpha_{zy} & \alpha_{zz} \end{bmatrix} \tag{2.16}$$

The mean polarizability, α_{iso} is a property observed when a molecule presents all orientations to the applied field and is given by

$$\begin{aligned} \alpha_{iso} &= \frac{1}{3}\left(\alpha_{xx} + \alpha_{yy} + \alpha_{zz}\right) \\ &= \frac{2}{3}\sum_{n\neq 0} \frac{\mu^2_{x,0n} + \mu^2_{y,0n} + \mu^2_{y,0n}}{\Delta E_{n0}} \end{aligned} \tag{2.17}$$

where α_{iso} is termed the *isotropic polarizability* given by the average of the diagonal elements of the polarizability tensor as indicated above. The numerator on the right hand side of Eq. 2.17 can be expressed as a scalar product of two vectors, $\mu_{0n} \cdot \mu_{n0}$. Hence, Eq. 2.17 becomes

$$\alpha_{iso} = \frac{2}{3}\sum_{n\neq 0} \frac{|\mu_{0n}|^2}{\Delta E_{n0}} \tag{2.18}$$

where

$$|\mu_{0n}|^2 = \mu_{0n} \cdot \mu_{n0} \tag{2.19}$$

Bibliography

[1] Yue Zhao, Guoxiong Yuan, Mario Leclerc and Philippe Roche, "A calorimetric study of the phase transitions in poly(3-hexylthiophene)", *Polymer Vol.* 36 No. 11, pp. 2211 2214, 1995.

[2] R. Mauer, M. Kastler, and F. Laquai, "The Impact of Polymer Regioregularity on Charge Transport and Efficiency of P3HT:PCBM Photovoltaic Devices", *Adv. Funct. Mater.*, 20, 2085-2092, 2010.

[3] Joyce M. Stout and Cliford E. Dykstra "Static Dipole Polarizabilities of Organic Molecules: Ab Initio calculation and a Perdictive Model" *J. Am. Chem. Soc.*, 117, 5127-5132, 1995.

[4] Petrucci, Ralph H., et al. "General Chemistry: Principles and Modern Applications", Upper Saddle River, NJ: Prentice Hall, 2007.

Chapter 3

Computer Simulation

In this chapter, an overview of computer simulation is given as well as a summary of the key ingredients necessary to carry out a molecular dynamics simulation, with particular emphasis on theoretical models, basis sets, force fields, optimization methods.

A computer simulation is an attempt to model a real-life or hypothetical situation on a computer so that it can be studied to see how the system works. By changing variables in the simulation, predictions may be made about the behavior of the system. Thus, it is a tool to virtually investigate the behavior of the system under study and often used as an adjunct to, or substitution for modeling systems for which simple closed form analytic solutions are not possible.

The two main families of simulation technique are molecular dynamics (MD) and Monte Carlo (MC); additionally, there is a whole range of hybrid techniques which combine features from both. The obvious advantage of MD over MC is that it gives a route to dynamical properties of the system: transport coefficients, time-dependent responses to perturbations, rheological properties and spectra.
The act of simulating something first requires that a model be developed; this model represents the key characteristics or behaviors of the selected physical or abstract system or process. The model represents the system itself, whereas the simulation represents the operation of the system over time. For effective simulation of an atomic system, certain properties of computations have to be understood and chosen correctly depending on the system to be modeled and simulated. These are theoretical models, basis sets and the type of calculations to be considered for a particular system.

3.1 Theoretical Models

A theoretical model is a way to mimic a system using a specific set of approximations. These approximations are combined with a calculation algorithm and are applied to atomic orbitals, defined by the basis set in order to compute molecular orbitals and energy The selection of the theoretical model depends on the size of the system and on the level of approximation.

In general, the methods can be separated into four main types namely, *semi-empirical, ab initio, density functional (DFT), and molecular mechanics (MM).*

Ab initio Methods

This method of computation is based only on theoretical principles, using no experimental data. It is the most popular type of models, despite the fact that the calculations take a long time. Examples are Hartree-Fock (HF), Moller-Plesset perturbation theory of Nth order(MPN) and Configuration Interaction (CI).

HF, Hartree-Fock is the basic *ab initio* model. It uses the approximation that the Coulombic electron-electron repulsion can be averaged, instead of considering explicit repulsion interactions (central field approximation). Here, it is the wavefunction that is used to compute the energy of the system. There are two ways to compute molecular orbitals using HF; UHF (unrestricted) or RHF (restricted). UHF uses a separate orbital for each electron, even if they are paired (mostly used for ions, excited states, radicals) whereas, RHF uses the same orbital spatial function for electrons in the same pair (good for species with paired electrons, no spin contamination).
One major drawback with Hartree-Fock level theory is the fact that it does not account for the so called correlation energy. The correlation energy is the energy which accounts for the fact that the electron does not move in an average field set up by all the other electrons, but feels the other electrons explicitly. One definition of the correlation energy is the difference between the exact solution of the Schrdinger equation and the sum of the Hartree-Fock and relativistic contribution;

$$E_{correlation} = E_{exact} - E_{Hartree-Fock} - E_{relativistic} \tag{3.1}$$

MPN, Moller-Plesset perturbation theory are denoted as MPn with $n = 2, \cdots, 6$. In practice, MP2 and MP4 are the only methods used, since the other ns (i.e n=3,5,6) are either too computationally expensive or do not significantly improve the results compared with a lower level of complexity.

CI, Configuration Interaction calculations are most often used for excited states. This calculation can be very accurate, but also very CPU expensive. CI is one the method used for correcting the absence of correlation energy in HF. It utilizes a theorem stating that, within the limits of the Born-Oppenheimer approximation (appendix) and classical quantum mechanics, inclusion of all possible excitation in the wave function will, at the limit of an infinite basis set, yield the exact energy. In CI, this is done by using a wave function which may be written as;

$$\psi = c_0\psi_0 + c_1\psi_1 + c_2\psi_2 + \dots \tag{3.2}$$

where ψ_0 is the wave function from HF-SCF and $\psi_{i>0}$ is the wave functions representing configurations which includes excitations. The coefficients c_0, c_1 etc., are found using the variational principle.
Generally, MPN and CI models start with an HF calculation and then correct for electron repulsion.

Semi-empirical Method

This method uses a certain number of experimental data throughout the calculation. For instance, bond lengths of a specific type will have a fixed value independent of the system (C=C bond will always be taken as 134 pm, for example). This speeds up computational time, but in general is not very accurate. Usually, semi-empirical methods are used for very big systems, since they can handle large amounts of calculation. ZINDO (Zerner's Intermediate Neglect of Differential Overlap) and AM1(Austin Model 1) are examples of semi-empirical of computation. ZINDO method was parametrized to reproduce electronic spectra while AM1 is a method that is most often used to model organic molecules.

Molecular Mechanics Method

This is the method for modeling giant systems. MM methods approximate atoms as spheres and bonds as springs. They use an algebraic equation for the energy calculation, not a wave function or electron density. The constants in the equation are obtained from experimental data or other calculations and are stored in a data library. The combination of constants and equations is called a *force field*. Examples of MM methods are UFF (Universal Force Field) – the method used in the `AVOGADRO` software by default, suitable for organic and inorganic molecules, and MMFF (Merk Molecular Force Field) a general-purpose model, used mainly with organic systems. The MMFF94 version of MMFF is used in `AVOGADRO`.

Density Functional Theory Density Functional Theory (DFT) differs from methods based on HF calculations in the way that it is the electron density that is used to compute the energy instead of a wave function. That is, the ground-state expectation value of any physical observable of a many-electrons system is a unique functional of the electron density, [n].
Mathematically,

$$\langle \Psi^0 | \hat{O} | \Psi^0 \rangle = O[n] \tag{3.3}$$

where n is the electron density of the system, O is a functional, Ψ^0 is the ground-state wavefunction, and $\hat{O}$ is a Hermitian operator.
The most popular DFT model is B3LYP (Becke, 3-parameter, Lee-Yang-Parr), which is known to be a hybrid, because, in addition to the corrections involving the density gradient, it also uses a fraction of the Hartre-Fock-like exchange terms.

3.2 Basis sets

A basis set in theoretical and computational chemistry is a set of functions (called basis functions which are combined in linear combinations generally as part of quantum chemical calculations to create molecular orbitals. These functions are typically atomic orbitals centered on atoms and theoretically, they can be any functions.

Molecular orbitals are computed using the selected theoretical model by linearly combining the atomic orbitals (since basis set describes the shape of atomic orbitals). Not all theoretical models require the user to choose a basis set to work with. The level of approximation of any calculation is directly related to the basis set used. Thus, the choice to make is a trade-off between accuracy of results and CPU time.
In the selection of a basis set, two types of basis functions can be considered; the Slater function, S(v) or the Gaussian function G(v). The difference between these two functions are illustrated in fig. 3.1.

Atomic orbitals, AOs can be described using either the Slater-type orbitals (STOs) or Gaussian-type orbitals (GTOs) or even both.

Slater-type orbitals (STOs)

These are functions used as atomic orbitals in the linear combination of atomic molecular orbital method. They posses exponential decay at long range (see figure) and *Kato's cusp condition* at short range (i.e., the analytical solutions of the stationary Schrdinger equation for one electron atoms). Unlike the hydrogen-like (*hydrogenic*) Schrdinger orbitals, STOs have no radial nodes.

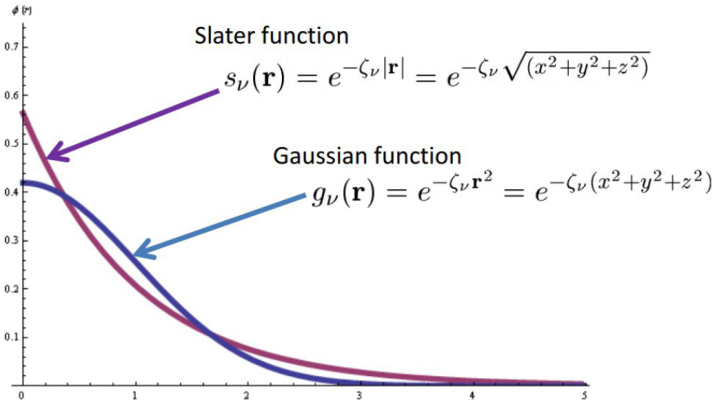

Figure 3.1: *Slater VS Gaussian type functions.*

Gaussian-type orbitals (GTOs)

GTOs are functions used as atomic orbitals in the linear combination of atomic orbitals (LCAO) method for the computation of electron orbitals in molecules and numerous properties that depend on these.

The principal reason for the use of Gaussian basis functions in molecular quantum chemical calculation is the *Gaussian Product Theorem* which guarantees that the product of two GTOs centered on two different atoms is a finite sum of Gaussians centered on a point along the axis connecting them.

The atomic orbitals are also described using both Slater STOs and GTOs. Though STOs describes the shape of atomic orbitals more closely, GTOs are mostly preferred because of their easier computational abilities. It is faster to compute several GTOs and combine them to describe an orbital than to compute one STO. This is why combinations of GTOs are commonly used to describe STOs, which in turn, describe atomic orbitals.

3.2.1 Types of Basis Set

In this section , three types of basis sets are discussed. These are minimal, split valence (also called Pople), and correlation-consistent basis set.

Minimal Basis Set

This type of basis set uses only one function for each atomic orbital. An example of such basis set is STO-nG ($n = 2, ..., 6$) which means that n GTOs are used to describe one STO, and only one STO is used to describe an atomic orbital (single Zeta). Since $n < 3$ gives too poor results, STO-3G

(ie STO-nG for n=3) is called the minimal basis set.

Split Valence Basis Set

This type of basis sets allow to specify the number of GTOs to use for core and valence electrons separately . These includes double Zeta (2 functions per atomic orbital) or triple Zeta. The notation for split valence basis set is K-LMG, where K is the number of sp-type inner shell GTOs, L is the number of inner valence s- and p-type GTOs, M is the number of outer valence s- and p-type GTOs and G indicates that GTOs are used .
Split valence basis set for organic molecules are called Pople. Examples of these are: 3-21G, 4-31G, 4-22G, 6-31G, 6-311G. Where, 6-311G for example implies, 6 GTOs for core orbital, 3 GTOs for inner valence, and 2 different GTOs for outer valence. 3-21G implies 3 GTOs for inner shell, 2 GTOs for inner valence, and 1 GTO for outer valence . These definitions apply to the others, the only difference is in the numbers.

Pople basis sets can be modified in two ways to obtain an approximation that better describes the system:

1. By letting the atomic orbitals distort from original shape (i.e., get polarized under the influence of the surroundings). Polarization can be added either as * or (d) or as (d,p) or **. For * or (d) type, d-type functions are added onto atoms other than Hydrogens and for (d,p) or ** type, p-type functions added on to Hydrogens, d-type functions added on to all other atoms, f-type functions added on to transition metals . Example of this type of Pople basis sets are 6-31G(d) or 6-31G**.

2. By letting the electron move far away from the nucleus, creating diffuse orbitals. This modification is useful when working with anions, excited states and molecules with lone pairs. Diffuse functions can be added as + (i.e. diffuse functions added on to atoms other than Hydrogens) or ++ (i.e. diffuse functions added on to all atoms) in front of the G. Example of this type of Pople basis sets is 6-31+G(d) or 6-31++G(d).

Correlation Consistent Basis set

All of the basis sets described until now were optimized at a Hartree-Fock level. However, it is legitimate to doubt that this optimization might not be the best for correlated computations. Dunning created a set of basis sets optimized using correlated wavefunctions. They are denoted as cc-pVXZ where, cc indicates that it is a correlation-consistent basis, pV indicates that it is a polarized valence basis and XZ indicates the zeta number (X= D for double, T for triple, Q for quadruple, 5,6,7) The prefix *aug-* can be used to add diffuse functions. Example cc-pVDZ or aug-cc-pVTZ [1].

3.3 Geometry Optimization

Unless an experimental geometry is available, the first step in a computational study is usually a geometry optimization to obtain an accurate structure of the molecule(s) of interest. Geometry optimization is the name for the procedure that attempts to find the configuration of minimum energy of the molecule. Implicit in the idea of a molecule is the concept of molecular structure. That is, a molecule is not only a collection of atoms but is a collection of atoms in a particular set of locations in space. Often, the structure of a molecule is of interest. Even if structure is less important, most important molecular properties are structure dependent. In the area of computational chemistry, structure determination is achieved through a geometry optimization.

The energy of a collection of N atoms as a function of their $3N - 6$ internal degrees of freedom is known as a potential energy surface (PES). Molecular structures correspond to minima on this surface. The function of a geometry optimization is therefore to find a minimum in the potential energy surface. Energy minimization is done when using either molecular mechanics (MM) or quantum mechanics(QM) methods, and it must precede any computational analysis in which these methods are applied. For example, geometry optimization can be used to:

- characterize a potential energy surface.
- obtain a structure for a single-point quantum mechanical calculation, which provides a large set of structural and electronic properties.
- prepare a structure for molecular dynamics simulation.

For the initial starting geometry, a single point energy (SPE) calculation is performed. The forces on the nuclei can be calculated from the wavefunction using the Hellmann-Feynman theorem (appendix). The force on a nucleus, I with position R_I is given by:

$$F_I = \langle \frac{\delta E}{\delta R_I} \rangle \tag{3.4}$$

where E is the energy. This force can then be used to find the ground state positions of the atoms and also used to calculate a molecular dynamics trajectory. As the forces point toward a (at least local) minimum in the energy, integrating the equations of motion for the nuclei will move the nuclei toward an equilibrium structure. This procedure can be rather time consuming with many SPE calculations needed to find the minima. Thus, it is common to

perform an initial energy minimization using molecular mechanics calculations to get to the vicinity of a minima and then perform a full *ab initio* geometry optimization.

In geometry optimization:

- An error, called the Pulay force [2], is introduced into the Hellman-Feynman forces if the basis set is incomplete. However, for a plane wave basis set, the wavefunctions do not depend on the nuclear positions, hence this error is zero as long as the electronic system has converged to the ground state.
- The nearest (in configuration space) point at which the forces are zero is found. Thus if a poor starting point is chosen, it may find a local rather than a global minimum in the potential energy surface or if the starting point is an energy maximum, it may remain there.

Computational chemistry programs useful for geometry optimization among others are Avogadro, Gaussian 09, LAMMPS and ORCA.

3.4 Force Fields

In the context of molecular modeling, a force field refers to the form and parameters of mathematical functions used to describe the potential energy of a system of particles (typically molecules and atoms).The usage of the term *force field* in chemistry and computational biology differs from the standard usage in physics. In chemistry, it is a system of potential energy functions rather than the gradient of a scalar potential, as defined in physics.

A force field is built up from two distinct components to describe the interaction between particles (typically atoms):

- the set of equations (called the potential functions) used to generate the potential energies and their derivatives, the forces.
- the parameters used in this set of equations.

There are three types of force fields:

- **all atom**–parameters provided for every single atom within the system.
- **united atom**–parameters provided for all atoms except non-polar hydrogens.

- **coarse grained**–an abstract representation of molecules by grouping several atoms into "super-atoms".

Functional Form
The basic functional form of a force field comprises both bonded terms relating to atoms that are linked by covalent bonds, and nonbonded (also called noncovalent) terms describing the long-range electrostatic and van der Waals forces. The specific decomposition of the terms depends on the force field, but a general form for the total energy in an additive force field can be written as

$$E_{total} = E_{bonded} + E_{non-bonded} \tag{3.5}$$

where the components of the covalent and noncovalent contributions are given by the following summations:

$$E_{bonded} = E_{bond} + E_{angle} + E_{dihedral} + E_{\omega} + \dots \tag{3.6}$$

The bond and angle terms are usually modeled as harmonic oscillators in force fields that do not allow bond breaking. E_{bond} comprises the energy for bond stretching, E_s and the energy for bond angle bending, E_b. E_{ω} is the torsional energy due to twisting about bonds; normally added to enforce the planarity of aromatic rings and other conjugated systems, and cross-terms that describe coupling of different internal variables, such as angles and bond lengths.

$$E_{non-bonded} = E_{electrostatic} + E_{vanderWaals} \tag{3.7}$$

The nonbonded terms are most computationally intensive because they include many more interactions per atom. A popular choice is to limit interactions to pairwise energies. The van der Waals term is usually computed with a Lennard-Jones potential and the electrostatic term with Coulomb's law. Nevertheless, both can be buffered or scaled by a constant factor to account for electronic polarizability and produce better agreement with experimental observations.

3.4.1 Force Field Development

The design of force fields for molecular mechanics is guided by by the following principles:

- Nuclei and electrons are lumped into atom-like particles.
- Atom-like particles are spherical (radii obtained from measurements or theory) and have a net charge (obtained from theory).

- Interactions are based on springs and classical potentials.
- Interactions must be preassigned to specific sets of atoms.
- Interactions determine the spatial distribution of atom-like particles and their energies.

Stretching and Bending

Considering the idea of a molecule to be a collection of masses connected by springs, then by applying Hooke's Law we can evaluate the energy required to stretch and bend bonds from their ideal values. Thus E_s and E_b may be expressed as:

$$E_s = \sum_{i=1}^{N} \frac{k_i^s}{2}(l_i - l_i^0)^2 \tag{3.8}$$

$$E_s = \sum_{i<j}^{M} \frac{k_{ij}^b}{2}(\theta_{ij} - \theta_{ij}^0)^2 \tag{3.9}$$

where N is the total number of bonds and M is the total number of bond angles in the molecule. k^s and k^b are the force constants for stretching and bending respectively. l_i and θ_{ij} are the actual bond lengths and bond angles. Finally, l_i^0 and θ_{ij}^0 are ideal bond lengths and bond angle s respectively.

It should however be noted that the formulation above (Eqs. 3.8 and 3.9) is only a first approximation. There are various factors which can be taken into account to improve the accuracy for these terms. These include noting that bond stretching requires more energy than bond bending and so for a molecule being deformed most of the distortion should occur in the bond angles rather than bond lengths. Another point to consider is that Hooke's Law overestimates the energy required to achieve large distortions. Another aspect is that as a bond angle gets compressed the two associated bond lengths become longer.

Torsion

Here, we consider the form of the E_ω term. The energy due to torsion is usually expressed in terms of a Fourier series:

$$E_\omega = \sum \frac{1}{2}[V_1(1 + \cos\omega) + V_2(1 + \cos 2\omega) + V_2(1 + \cos 3\omega) + \dots] \tag{3.10}$$

where the sum is over all unique sequences of bonded atoms, ω is the torsion angle, and V_1, V_2, V_3, are the adjustable parameters. In general, the series is truncated at the third term, with V_1, V_2 and V_3 chosen so that the resultant

conformation agree well with experiment for a given group of molecules.

Non bonded Interactions

The final term contributing to E_{total} is the energy from pairwise non bonded interactions. Such interactions are modeled by London dispersion forces (for the attraction) and van der Waals forces (for the repulsion). Some of the common potential functions implementing the above are the Lennard Jones (V_{LJ} and Buckingham (V_{Buck}) potentials [3],

$$V_{LJ} = \frac{A}{r^{12}} - \frac{B}{R^6} \tag{3.11}$$

where $A = 4\epsilon\sigma^{12}$ and $B = 4\epsilon\sigma^6$. ϵ, the well depth and σ, the diameter are parameters in the model which are normally found by experiments.

$$V_{Buck} = A' exp(\frac{B'}{r}) - \frac{C}{R^6} \tag{3.12}$$

An important non bonded energy term that is always taken into account is the electrostatic interaction. Typically the electrostatic interaction dominates the total energy of a system by a full magnitude. The electrostatic contribution is modeled using a Coulombic potential,

$$E_{Coul} = \sum_{ij=1} \frac{q_i q_j}{4\pi\epsilon_0 r_{ij}} \tag{3.13}$$

The electrostatic energy is therefore said to be a function of the charge (q) on the non-bonded atoms, their interatomic distance, (r_{ij}) and a molecular dielectric expression that accounts for the decrease of electrostatic interaction due to the environment (such as by solvent or the molecule itself). ϵ_0 is the permittivity of free space.
The accuracy of the electrostatic term depends on the correct assignment of charges to individual atoms.

Generality is still a problem with force fields, though with the development of the Universal Force Field (UFF) an attempt has been made to develop a generalized force field applicable to a large portion of the periodic table and not be restricted to particular groupings of atoms such as proteins, nucleic acids etc. other force field developed so far are AMBER, OPLS, MMFF, GROMOS, CHARMM, MM3, etc. AMBER, OPLS and CHARMM are geared more to larger molecules (proteins, polymers) in condensed phases.

Bibliography

[1] Anna Tomberg, "Gaussian 09W Tutorial:An Introduction to Computational Chemistry Using G09 and Avogadros Software".

[2] H. Bernhard Schlegel, Perspective on "Ab initio calculation of force constants and equilibrium geometries in polyatomic molecules. I. Theory" *Theor. Chem. Acc.*, 103:294-296, 2000.

[3] Rajarshi Guha (9915607) and Rajesh Sardar (9915610), "Force Fields in Molecular Mechanics", 2001.

Chapter 4

MD Simulation of Poly(3-hexylthiophene)

In this chapter, we give an account and details of the computational methods and procedures used in simulating $(P3HT)_n$. Simulation results are also analyzed and discussed in this part.

4.1 Development of P3HT Molecular Structure and Geometry Optimization

P3HT, because of its polymeric nature can have as many units as possible depending on the purpose for which it is being considered for. This is the reason why as shown in Fig. 2.1 (Chapter Two), there is an n parameter assigned to its chemical structure which denotes the number of repeat units. The main structure considered in this work is the RR-P3HT molecular structure as shown in Fig., 2.3 (Chapter Two). Avogadro Chemistry software was used to draw the molecular structures of RR-P3HT at n = "0", 1, 2 and 3 (where n=0 is the structure obtained when the hexyl side chain is absent – Thiophene) after which, each unit was optimized using molecular mechanics force field, MMFF94 (the program, `AVOGADRO` uses this field by default). Figure 4.1 shows snapshots of the various optimized RR-P3HT molecular units drawn using `AVOGADRO`. The main purpose for using `AVOGADRO` was to generate inputs for *ab initio* geometry optimization.

Details of the Gaussian 09W runs performed are as follows:

- The Thiophene group of the single unit P3HT, two, three, four and five units RR-P3HT were all optimized at B3LYP/6-311G** level.

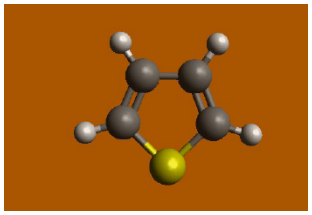

(a) Thiophene ($n = 0$) Before optimization

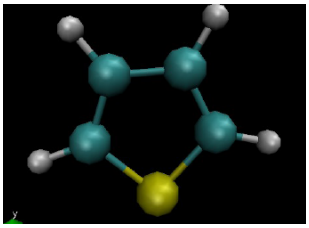

(b) $n = 0$; After optimization at B3LYP/6-311G**

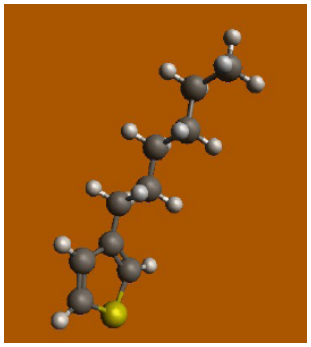

(c) $n = 1$; Before optimization

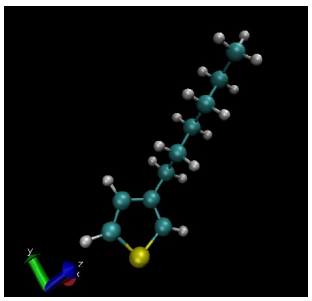

(d) $n = 1$; After optimization at MP2/6-311++G**

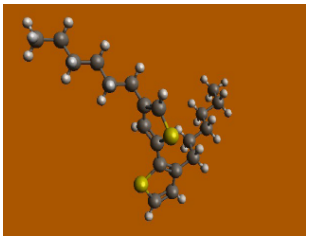

(e) $n = 2$; Before optimization

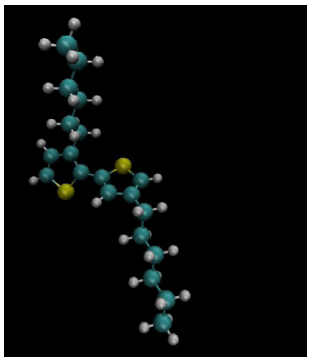

(f) $n = 2$; After optimization at B3LYP/6-311G**

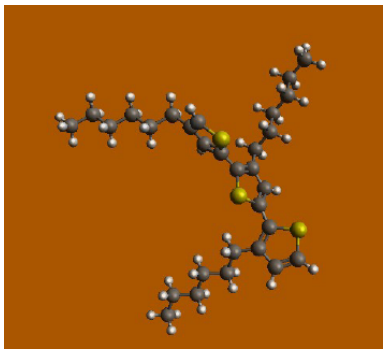

(g) $n = 3$; Before optimization

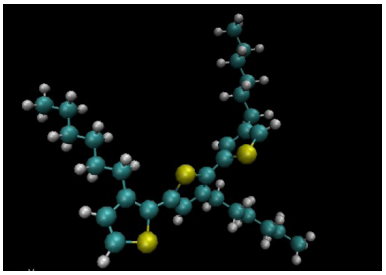

(h) $n = 3$; After optimization at B3LYP/6-311G**

Figure 4.1: *Developed molecular structures of RR-P3HT before (a, c, e and g) and after (b, d, f and h) optimization for n="0", 1, 2 and 3. AVOGADRO chemistry software was used to draw these structures while Gaussian 09W was used for the geometry optimization .*

- Single unit P3HT, ($P3HT_1$) was optimized at B3LYP/6-311G**, MP2/6-311G** and finally at MP2/6-311++G** level where both diffuse and polarization functions were added. Here, the last configuration of the B3lYP/6-311G** output was used for the optimization at MP2/6-311G** level and that of MP2/6-311G** was used for the optimization at MP/6-311++G** level (the `MOLDEN` software was used to write out the xyz files in each case). Table **4.1** shows the final configuration obtained for ($P3HT_1$) (in the form of xyz coordinates).

Table 4.1: *Final Configuration of Single Unit P3HT at MP2/6-311++G** level.*

Site Label	x [$\mathring{A}$]	y [$\mathring{A}$]	z [$\mathring{A}$]
C2	-8.212795	0.120778	1.977662
C2	-7.183835	-0.478962	2.761079
C3	-6.462647	0.209933	3.885691
H3	-5.577404	-0.374814	4.165464
C4	-7.361889	0.388901	5.117005
H3	-6.105028	1.192907	3.551427
H3	-7.711991	-0.599235	5.443853
H3	-8.255581	0.958956	4.830522
C4	-6.655102	1.094389	6.274135
H3	-5.760030	0.521823	6.554919
C4	-7.549250	1.266087	7.502199
H3	-6.305705	2.080936	5.938712
H3	-7.897685	0.278702	7.835667
H3	-8.445777	1.834954	7.218795
C4	-6.852679	1.972864	8.665535
H3	-5.958076	1.402648	8.946518
C5	-7.763291	2.136842	9.883135
H3	-6.504307	2.957593	8.328802
H4	-8.102036	1.161131	10.246780
H4	-8.650362	2.725040	9.625961
H4	-7.248558	2.643593	10.705024
C1	-8.762311	-0.748236	1.054831
H2	-8.531295	1.153516	2.081968
C1	-6.989671	-1.803083	2.404457
S	-8.034338	-2.297598	1.138416
H1	-9.544447	-0.551841	0.332971
H1	-6.279472	-2.502067	2.829273

Table 4.2: *Computed polarizability values of various RR-P3HT units (i.e., n = 0, 1, 2, 3) at B3LYP/6-311G** level and the corresponding calculated isotropic polarizabilities (α_{iso}).*

n	α_{xx} [au]	α_{yy} [au]	α_{zz} [au]	α_{iso} [au]	Mw / Da
0	62.7855686	68.7846736	28.9453006	53.505	84.140
1	106.1531186	128.7884609	148.8326913	127.925	168.300
2	309.6419217	267.5317679	224.9396554	267.371	334.585
3	392.3234599	430.3369819	422.5938854	415.085	501.878

After each of the optimization, the static polarizability was computed by Gaussian 09W (see table **4.2** below) from which the corresponding isotropic polarizability (Eq. 2.17 in Chapter Two) was determined.

4.2 Molecular Dynamics Simulation

Among all the structures optimized, the single unit P3HT molecule was used for the MD simulation where the starting geometry (Figure 4.2a) for the simulation was created using Packmol computer program with xyz coordinates taken from the last configuration at the MP2/cc-pvtz level which is slightly different from the geometry optimized at the MP2/6-311++G** level (table **4.1**). In developing the starting geometry, $n = 50$ monomers of single unit P3HT, $(P3HT)_1$ molecule were placed in a box of length 23.327428 $\mathring{A}$ (calculations shown in Appendix). This was viewed using VMD visualization software (Fig. 4.2b.). With the starting geometry developed, MD simulations (using DL_POLY classic software) were performed using the OPLS-AA force field for 50 monomers of $(P3HT)_1$ in a cubic box of length 23.327428 $\mathring{A}$. Lennard Jones (LJ) and Coulombic parameters (i.e., LJ distance σ_{ij}, LJ interaction strength ϵ_{ij} and charge q_i, Eq. 4.1) from OPLS-AA model used was adapted from Ref., [2]. The combination rules chosen for the LJ parameters is shown in the Appendix.

OPLS-AA force field for the non-bonded interaction (E_{ab}) between any two atoms **a** and **b** is of the form [1]:

$$E_{ab} = \sum_{i}^{on\mathbf{a}} \sum_{j}^{on\mathbf{b}} \left[\frac{q_i q_j e^2}{r_{ij}} + 4\varepsilon_{ij} \left[\left(\frac{\sigma_{ij}}{r_{ij}} \right)^{12} - \left(\frac{\sigma_{ij}}{r_{ij}} \right)^{6} \right] \right] f_{ij} \qquad (4.1)$$

Where r_{ij} is the interatomic separation (distance), e, electron charge and f_{ij} is a constant of value 0.5 if i, j are 1, 4 respectively, otherwise, $f_{ij} = 1.0$.

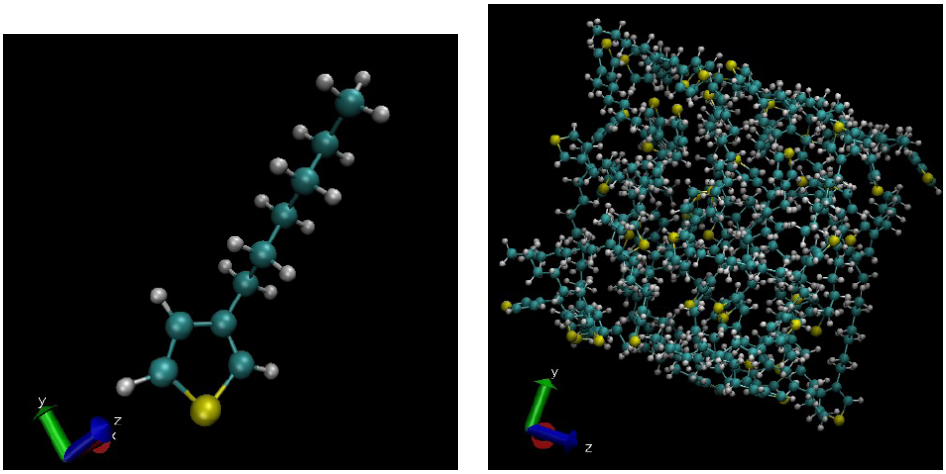

(a) Optimized single unit for MD

(b) Starting geometry for MD simulation

Figure 4.2: *Snapshots of the optimized* ($P3HT_1$) *structure at MP2/6-311++G** level,(a) and the starting geometry for the MD simulation consisting of 50 monomers.*

Atom types considered for this model is shown in Fig. 4.3 below. Table **4.3** shows the non-bonded parameters used in the atomistic simulation of $(P3HT)_1$.

The system was then studied by performing 1000 ps-long MD run at different temperatures with an initial temperature of 300 K to 360 K at intervals of 20K, then from 360 K to a maximum of 760 K at intervals of 100 K. The following settings were made to control the system at each temperature; timestep at 0.002 ps, equilibration at 50 ps, sampling done at NVT ensemble with Hoover-Nose thermostat was used with relaxation constant 0.5 ps, Ewald summation was used to approximate the long range electrostatic contributions the intermolecular van der Waals forces cutoff was implemented at 10.0 $\mathring{A}$. After each run, the radial distribution function, RDF (Appendix) data was extracted and plotted. Figures 4.5-4.10 show the radial distribution functions (at different temperatures) for C1-C1, C2-C2, C3-C3, C4-C4, C5-C5 and S-S atomic pairs considered for the non-bonded interaction using figure 4.3.

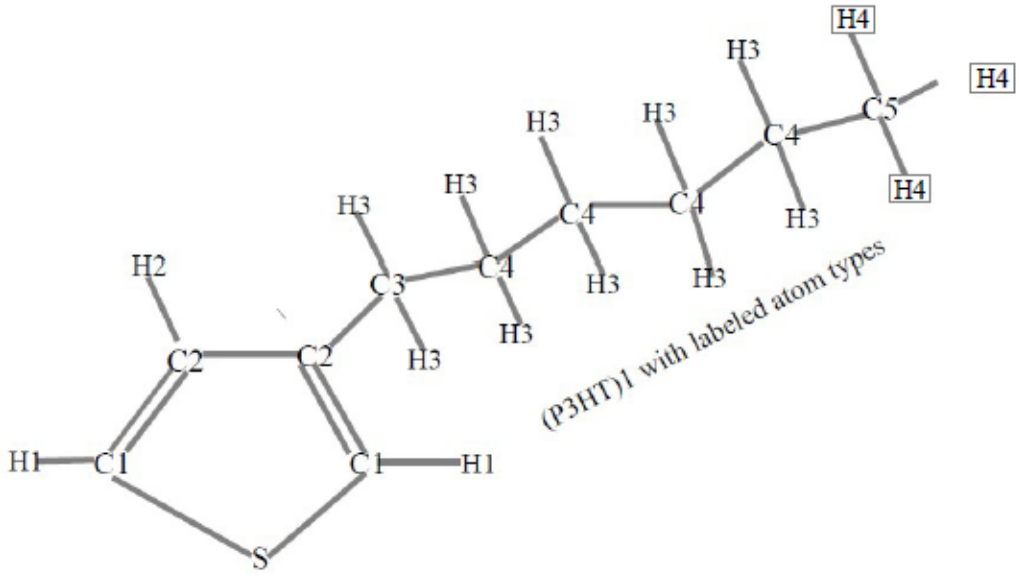

Figure 4.3: *Chemical structure of single unit P3HT. Atoms of different type for the OPLS-AA model are labelled with different numerical suffixes (i.e., 1, 2, 3, 4 and 5).*

4.3 Results and Discussions

Table **4.2** shows a substantial increase in the molecular polarizability as we increase the number of molecular units (i.e., for RR-P3HT). This was observed when the isotropic polarizability was plotted as a function of the number of molecular units (figure 4.2(a)) where from $n = 0$ to $n = 1$, a gradual change in polarizability is seen as a consequence of the absent hexyl chain contrary to the sharp rise observed in the presence of the hexyl chain from $n = 1$ to $n = 3$.

Figure 4.2(b) emphasizes the fact that as the system is elongated by the addition of more monomer chains, the electrons are able to move more easily increasing their polarizability. In contrast, small molecules (for example $n = 0$, Fig. 4.1(b)) are less polarizable (Fig. 4.2(a) and 4.2(b)).

In all, Fig. 4.2 shows that the system becomes more polarizable as the number of monomer chains increases. This is evident in figure 4.2(c) where we see a linear increase of polarizability with an increase in the molecular weight of the ($P3HT_n$) system. It is however not clear whether the linear trend observed in figures 4.4(a) and 4.4(b) above would continue or decline beyond $n = 3$.

For the RDFs (figures 4.5-4.10), a common feature is the peak around r

Table 4.3: *Non-bonded parameters (OPLS-AA model) used in atomistic simulation models of* $(P3HT)_1$.

Atom type i	$\sigma_{ii}[\mathring{A}]$	ε_{ii} [kcal/mol]	$q_i[e]$
S	3.5500	0.2500	-0.1496
C1	3.5500	0.0700	-0.1496
C2	3.5500	0.0700	-0.1817
C3	3.5000	0.0600	0.0617
C4	3.5000	0.0600	-0.1200
C5	3.5000	0.0600	-0.1800
H1	2.4200	0.0300	0.21600
H2	2.4200	0.0300	0.1817
H3	2.5000	0.0300	0.0600
H4	2.5000	0.0300	0.0600

= 4.5 , which corresponds to the separation between monomers on the same chain. Another feature observed in all is the absence of peaks at **r** less 2.5 $\mathring{A}$ which shows that there is essentially zero probability of finding particles at distances less than 2.5 $\mathring{A}$ from each other. This is due to the presence of very strong repulsive forces at short distances. At long range, the RDFs are expected to tended to the value of 1 as can be observed in figure 5 which confirms the fact that RDF describes the average density at this range. The occurrence of peaks at temperatures of 300 K, 320 K, 340 K and 360 K at long range however, implies high degree of ordering in P3HT molecule as seen clearly in figures 4.6(a), 4.7(a) and 4.10(a). This confirms the semi-crystalline nature of P3HT where it becomes less amorphous. Another feature observed that at high temperatures, (around 460 K to 760 K) is the widening and vanishing of peaks (figures 4.5(b), 4.8(b), 4.9(b) and 4.10(b)) indicating a change in the condense phase (from semi-crystalline back to amorphous) in the material. This represents a less welldefined molecular structure (increased disorder) at high temperatures which is in agreement with Cheung et al., 2009b [3] for low molecular weight P3HT. The slight shift observed in the peaks (Fig. 4.10) with temperature could be attributed to the expansion of the side chain (alkyl chain) as the temperature is increased. This sidechain disorder directly affects the molecular packing, which influences the morphology and would affect the charge mobility.

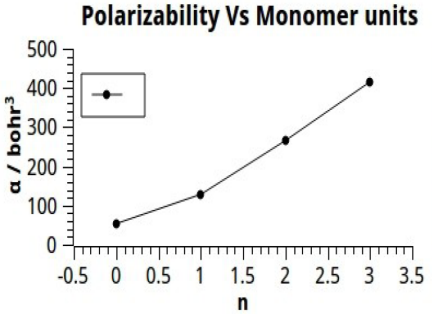

(a) Variation of polarizability with n molecular units

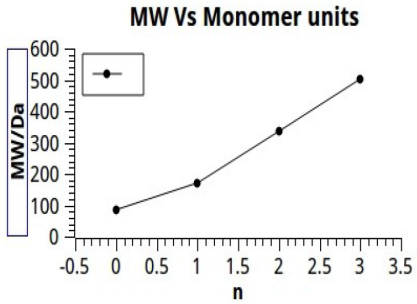

(b) Variation of molecular weight (Mw) with n molecular units

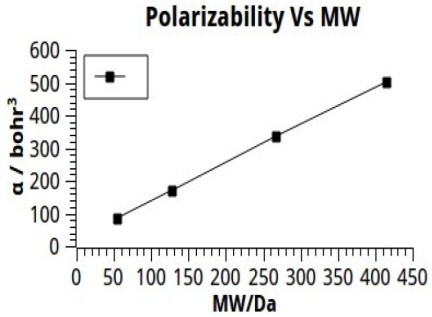

(c) Plot of Polarizability Vs Molecular weight

Figure 4.4: *(a) shows the variation of polarizability with the number of molecular units, n. (b) A plot of polarizability as a function of the calculated Molecular weight (MW) for the various molecular units developed (i.e., n=0, 1, 2 and 3) and (c) shows a plot of the MW as a function of the number of molecular units.*

4.4 Development of Ab Initio Polarizable Force Fields for $(P3HT)_1$

We have also developed force fields from *ab initio* data with and without the inclusion of explicit molecular polarizability. This was carried out for $(P3HT)_1$ optimized at the MP2/cc-pvtz level where "cc-pvtz" refers to Dunning's correlation consistent basis set. [4] The geometry obtained differs slightly from the B3LYP/6-311++G** one as shown below: With this geometry we developed an *ab initio* force field for a single monomer of P3HT, $(P3HT)_1$, by taking the following:

- Obtain the partial charges on the atoms – these were determined to re-

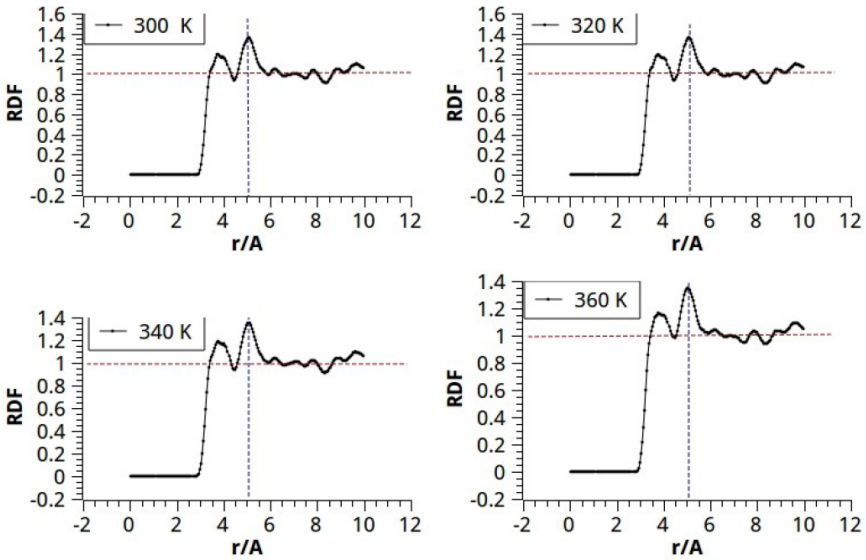

(a) At $T = 300$ K to $T = 360$ K

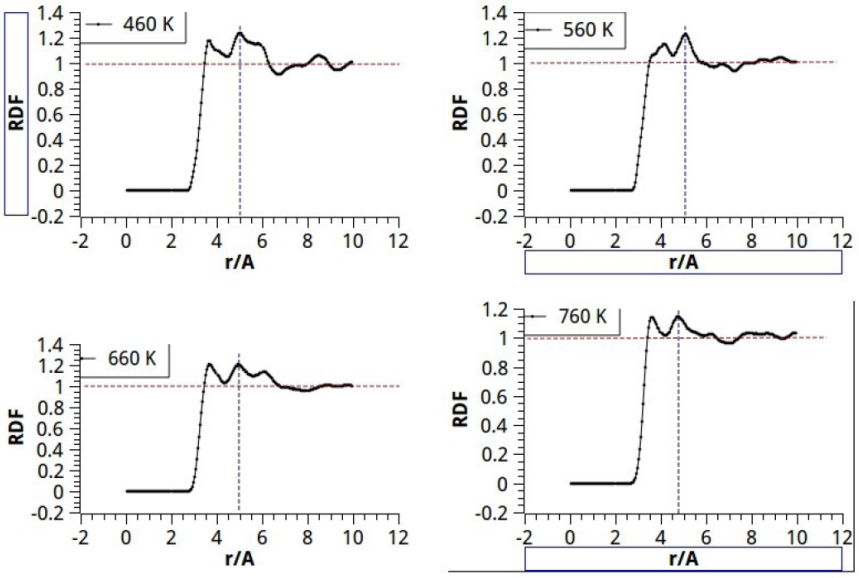

(b) At $T = 460$ K to $T = 760$ K

Figure 4.5: *Atomic radial distribution function for C1-C1 interaction at different temperatures (T).*

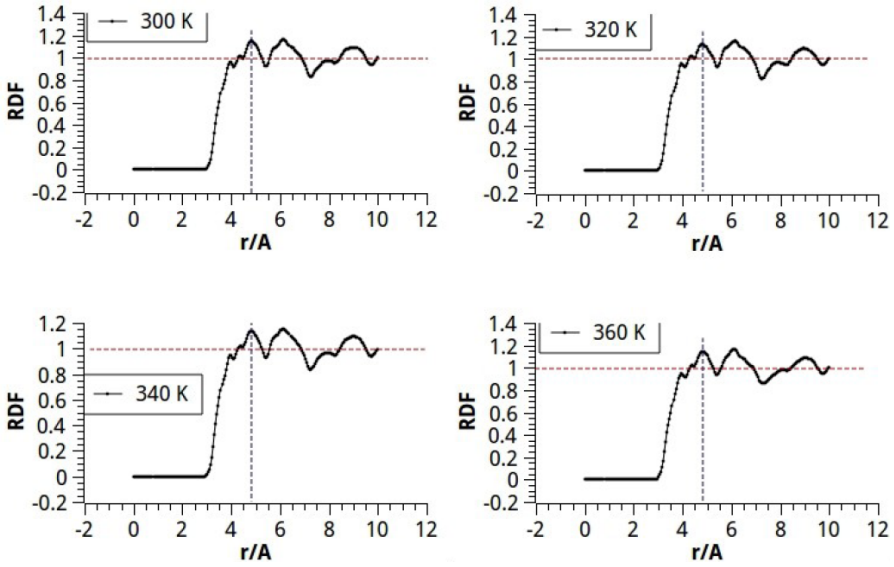

(a) At $T = 300$ K to $T = 360$ K

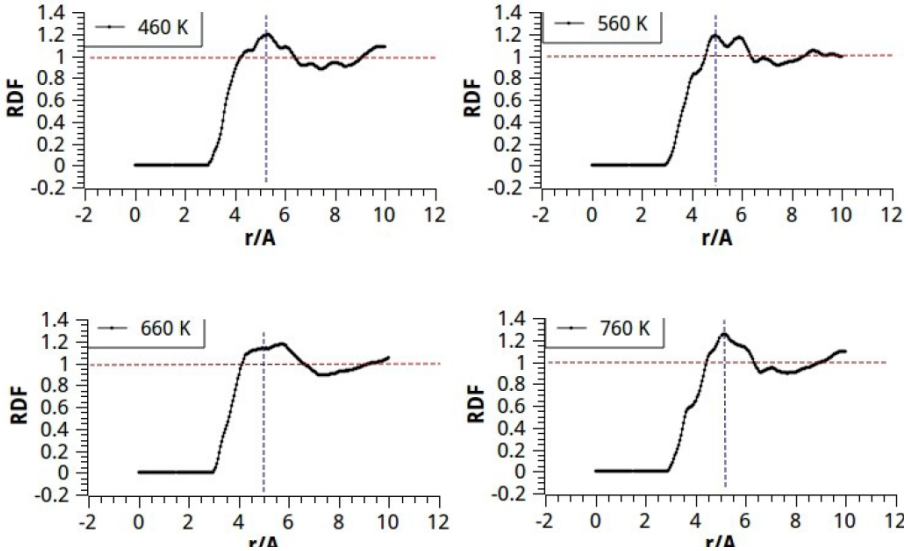

(b) At $T = 460$ K to $T = 760$ K

Figure 4.6: *Atomic radial distribution function for C2-C2 interaction at different temperatures (T).*

produce the first two electrostatic multipole moments of the molecule in its equilibrium position and the *ab initio* electrostatic potential around the molecule.

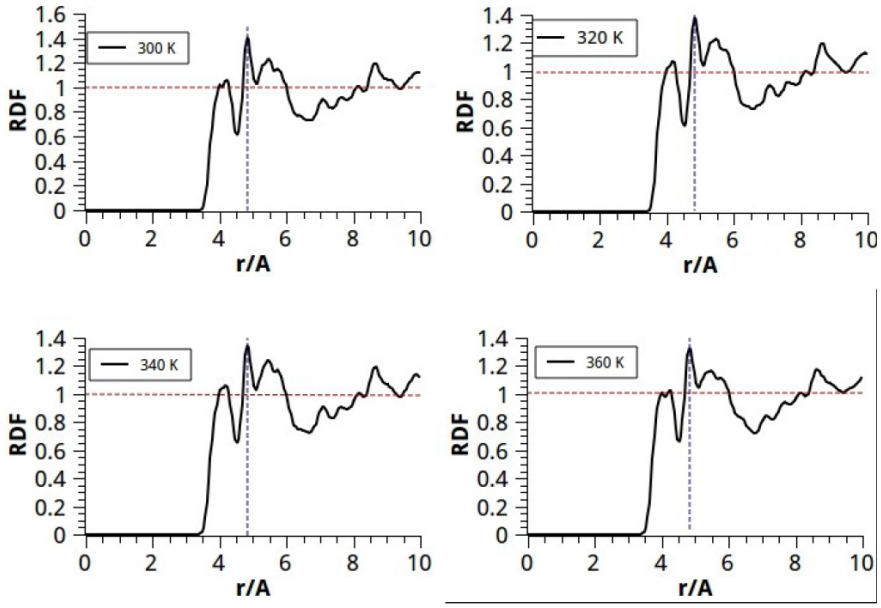

(a) At $T = 300$ K to $T = 360$ K

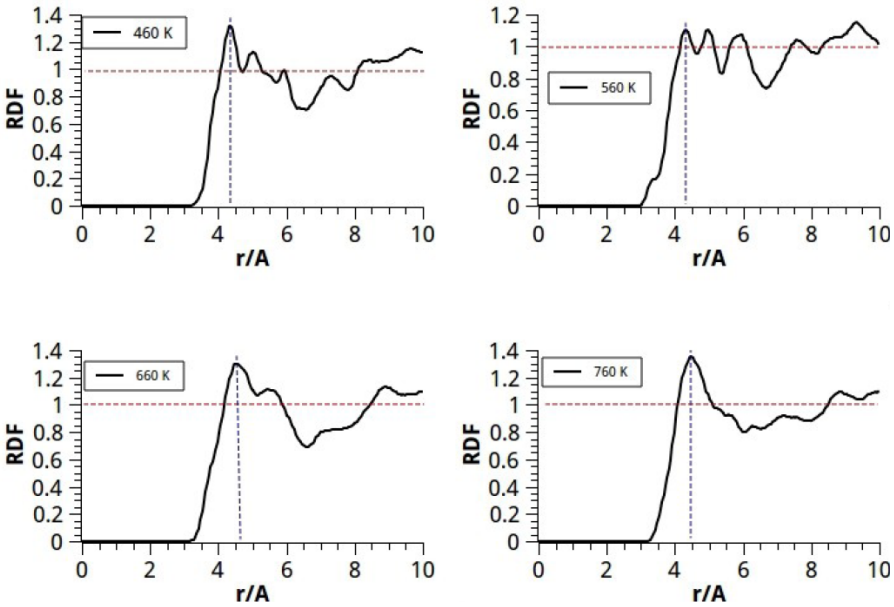

(b) At $T = 460$ K to $T = 760$ K

Figure 4.7: *Atomic radial distribution function for C3-C3 interaction at different temperatures (T).*

- Determine the distributed polarizabilities – by reproducing the induced

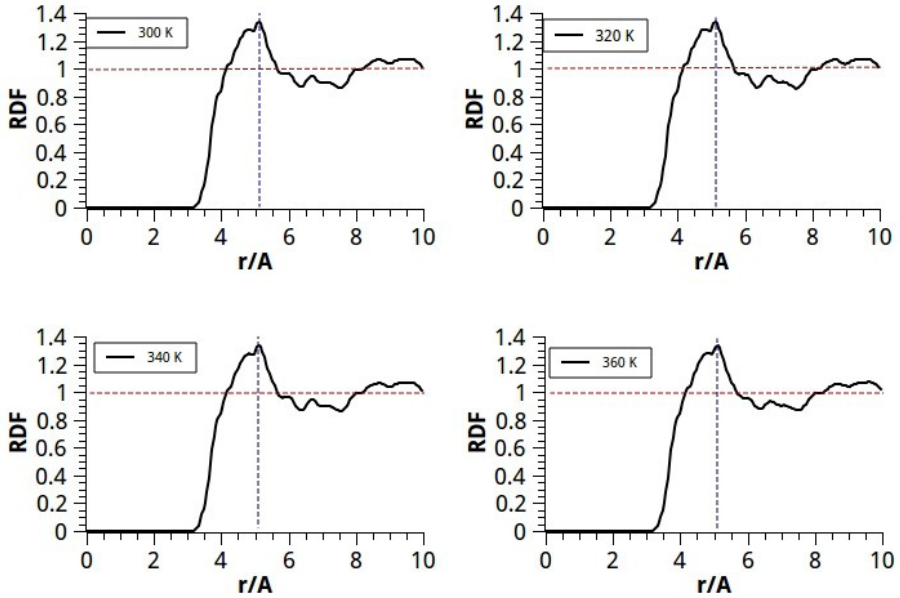

(a) At $T = 300$ K to $T = 360$ K

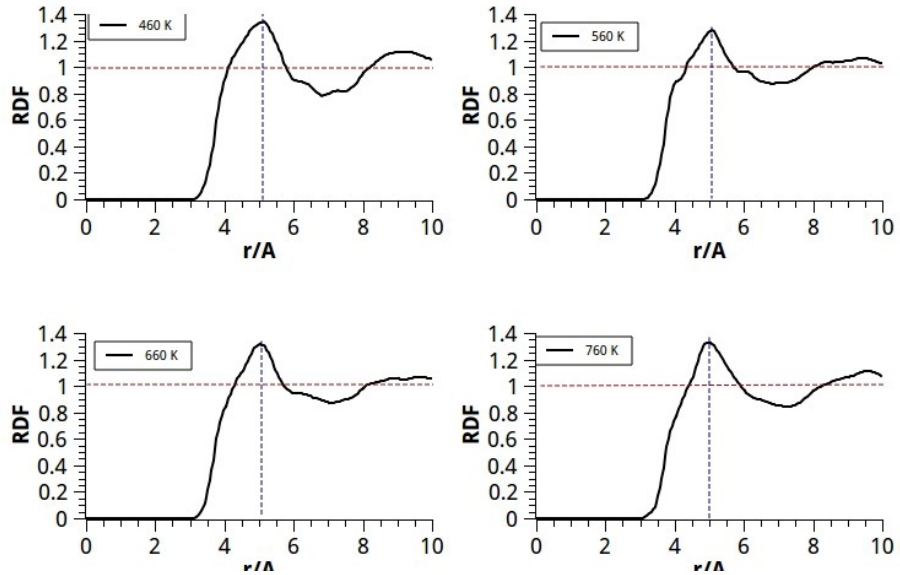

(b) At $T = 460$ K to $T = 760$ K

Figure 4.8: *Atomic radial distribution function for C4-C4 interaction at different temperatures (T).*

dipole moments for dimers of $(P3HT)_1$.

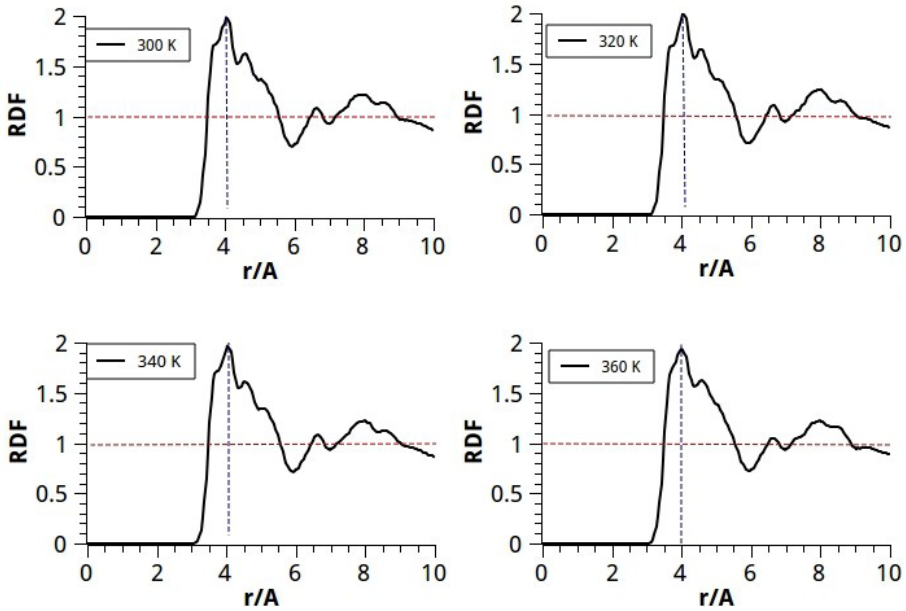

(a) At $T = 300$ K to $T = 360$ K

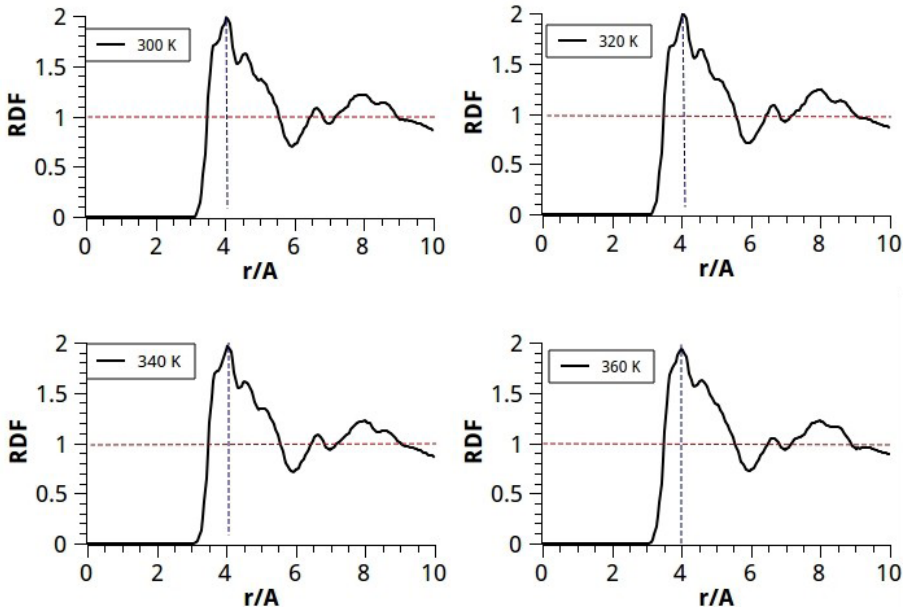

(b) At $T = 460$ K to $T = 760$ K

Figure 4.9: *Atomic radial distribution function for C5-C5 interaction at different temperatures (T).*

- Parameterize the Lennard-Jones pairwise potential – in order to re-

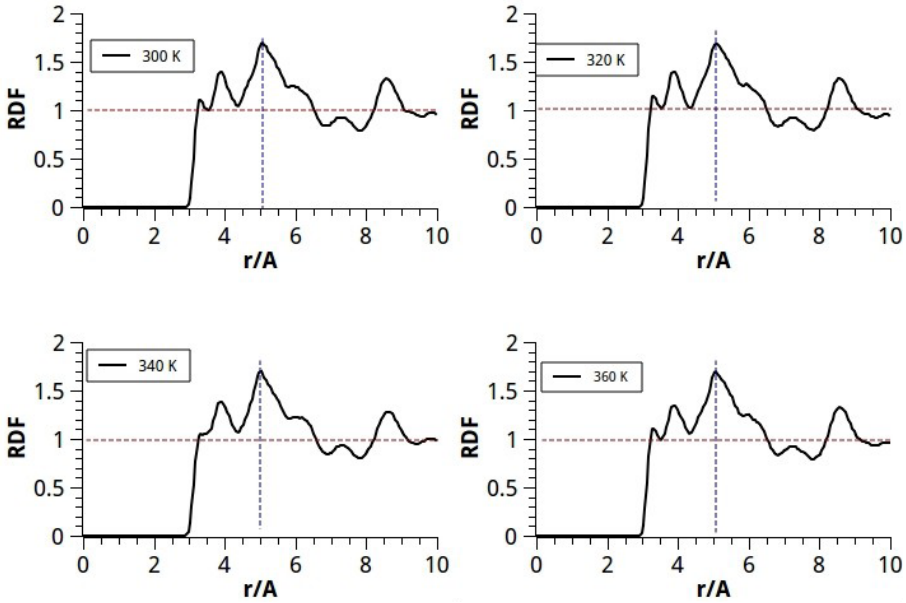

(a) At $T = 300$ K to $T = 360$ K

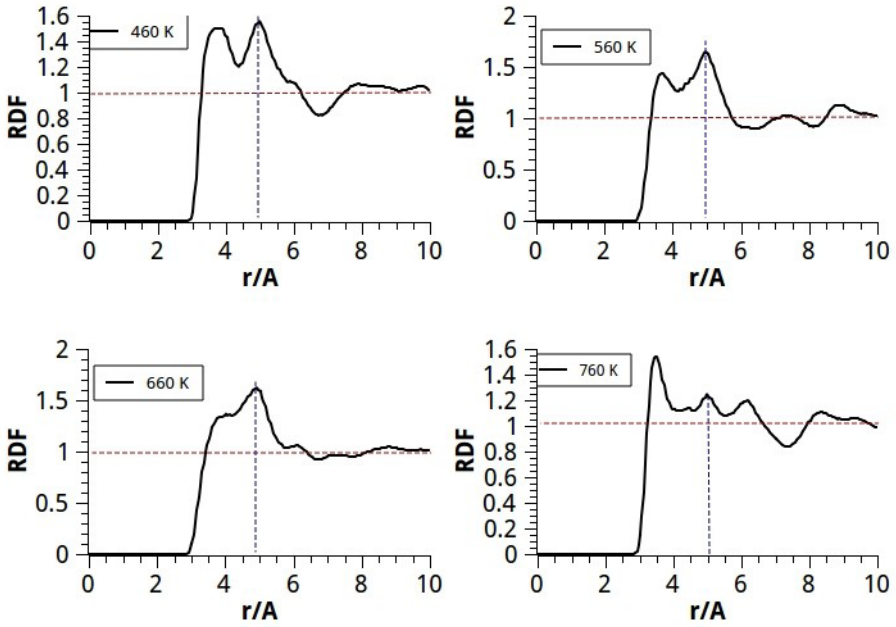

(b) At $T = 460$ K to $T = 760$ K

Figure 4.10: *Atomic radial distribution function for S-S interaction at different temperatures (T).*

produce the *ab initio* net forces and torques about the centres-of-mass

Table 4.4: *Optimized geometry of (P3HT)$_1$ with MP2/cc-pvtz*

Site Label	x [Å]	y [Å]	z [Å]
S	-4.042862	-0.242139	-0.696343
C1	-3.533777	1.236194	-0.000108
C2	-2.287393	1.116301	0.570613
H3	-1.787534	1.935376	1.068338
C2	-1.738174	-0.185670	0.445753
C3	-0.377297	-0.577186	0.934529
C1	-2.596555	-1.029400	-0.229475
H1	-2.442695	-2.069914	-0.466082
H1	-4.169992	2.104413	-0.039904
C4	0.738369	-0.004156	0.058889
H3	-0.295233	-1.665761	0.957415
H3	-0.240518	-0.228580	1.961256
H3	0.600587	-0.358404	-0.965831
C4	2.128241	-0.381648	0.552942
H3	0.644432	1.084238	0.024465
H3	2.216211	-1.471418	0.588127
H3	2.255279	-0.028785	1.580517
C4	3.242873	0.185519	-0.315912
H3	3.114489	-0.166123	-1.343636
C4	4.635444	-0.190372	0.173254
H3	3.154973	1.275249	-0.350825
H3	4.720929	-1.278828	0.207356
H3	4.761049	0.161040	1.199877
C5	5.737444	0.385256	-0.706438
H4	5.642076	0.025295	-1.730718
H4	6.726852	0.108778	-0.345611
H4	5.682662	1.473446	-0.732329

torques for molecules in the dimers of (P3HT)$_1$.

4.4.1 *Ab Initio* Atomic Partial Charges

In order to obtain the atomic partial charges on the (P3HT)$_1$ monomer, the electrostatic potential was calculated at the MP2/cc-pvtz level on a grid of points surrounding the molecule in its equilibrium position. The grid of points was chosen according to the Merz-Singh-Kollman scheme [5]. A total

of $N_V = 1199$ points were used. As in other parts of this work, the resolution-of-identity method (also called "density fitting") as programmed in the `ORCA` code was used to speed up the MP2 calculations. The atomic partial charges were fitted to reproduce the MP2/cc-pvtz *ab initio* dipole moment and the electrostatic potential while enforcing charge neutrality by minimizing the following quantity:

$$\chi^2_{\text{ch}} = \sum_{i=1}^{N_V} \left[V_i^{\text{model}} - V_i^{ai}\right]^2 + \lambda_{\text{dipole}} \left[\vec{\mu}_{\text{model}} - \vec{\mu}_{ai}\right]^2 + \lambda_{\text{charge}} Q^2 \qquad (4.2)$$

where, V_i^{model} and V_i^{ai} are the electrostatic potentials at the grid point i from the model and from the *ab initio* MP2 calculations, respectively. $V_i^{\text{model}} = \sum_a^{N_c} q_a / r_{ai}$ is the electrostatic potential from a point-charge model with $\{q_a\}$ as the set of all N_c charges on the molecule and r_{ai} is the distance from site a on the molecule to point i of the grid. $N_c = 27$ is the number of charged sites on the molecule. In this case, only atomic sites were used. The dipole moment of the model was obtained from: $\vec{\mu}_{\text{model}} = \left(\sum_a^{N_c} q_a x_a, \sum_a^{N_c} q_a y_a, \sum_a^{N_c} q_a z_a\right)$ and the total charge $Q = \sum_a^{N_c} q_a$, where, (x_a, y_a, z_a) is the position of the ath site of the molecule. The charges obtained from minimizing Eq.2 above are given in the Table below: The result-

Table 4.5: *Ab initio* Partial Charges

Site Label	Charge [au]
S	0.06460636
C1	-0.29788095
C2	-0.05807258
C3	0.14605419
C4	0.05166622
C5	-0.03451569
H1	0.21158131
H2	0.10230740
H3	-0.2100013
H4	0.00454286
Total	0

ing dipole moment is $(0.7739, 0.0949, 0.2783)$ Debye yielding a total dipole moment of 0.8279 Debye which compares well with the *ab initio* values of

$(0.7740, 0.0948, 0.2783)$ Debye and 0.8280 Debye, respectively. The root-mean-square error (RMSE) of the fit to the electrostatic potential was 0.0029 au which is much smaller than the root-mean-square (RMS) value (0.029 au) of the electrostatic potential of the grid points.

It is not clear to us why sulphur (S) has a positive charge or why the hydrogen atoms labelled H3 have negative charges. One would have expected S, being the most electronegative element in the set, to have a negative charge. In the same way, one would expect all the hydrogen atoms to have positive charges. However in view of the fact that we have not included point dipole moments in our model, it is possible that the inclusion of such point dipole moments will lead to a situation in which the partial charge on S is negative and that on every H is positive as expected.

4.4.2 *Ab Initio* Distributed Polarizabilities

Having obtained the atomic partial charges, we proceeded to determine the polarizabilities. Although, in comparison with other molecules, $(\text{P3HT})_1$ has a modest sized dipole moment, its MP2/cc-pvtz dipole-dipole polarizability α tensor has large values of (162.87987, 116.55362, 101.17242, −1.05911, 13.37494, 5.07430) au for $(\alpha_{xx}, \alpha_{yy}, \alpha_{zz}, \alpha_{xy}, \alpha_{xz}, \alpha_{yz})$. Its diagonalized tensor is $(\alpha_{xx}, \alpha_{yy}, \alpha_{zz}) = (97.02241, 117.92937, 165.65413)$ au with an isotropic value of $\alpha_{\text{iso}} \equiv (\alpha_{xx} + \alpha_{yy} + \alpha_{zz})/3.0 = 126.8686$ au.

We determined the atomic polarizabilities to reproduce the induced dipole moment $\vec{\mu}_{\text{ind}}$ of the dimer, i.e., $\vec{\mu}_{\text{ind}} = \vec{\mu}_{AB} - \vec{\mu}_A - \vec{\mu}_B$, where $\vec{\mu}_{AB}$ is the dipole moment of a dimer of $(\text{P3HT})_1$ molecules, and $\vec{\mu}_A = \vec{\mu}_B$ are those of the monomers A and B. Spherical atomic polarizabilities were placed only on the heavy atoms (i.e., all atoms except H) and their values determined to reproduce the induced dipole moments of 89 dimers chosen from snapshots of MD simulations as described below. The popular Drude model has been used to obtain the induced dipole moments of the model with charges of magnitude 8.0 au on each "core" and "shell."

The total polarizability obtained in the fit was 120.6338 au which is only 5% less than the isotropic *ab initio* value of 126.8686 au. Increasing the magnitude of the core-shell charges did not lead to any change in the distributed polarizabilities to 4 decimal places. The distributed polarizabilities obtained are listed below:

4.4.3 *Ab Initio* Lennard Jones parameters

The Lennard-Jones (LJ) parameters ϵ_{aa} and σ_{aa} describing the interaction between identical sites were determined by fitting to the centre-of-mass torques

Table 4.6: *Ab Initio* Distributed Polarizability

Site Label	Polarizability [au]
S	2.06086
C1	1.93629
C2	1.07356
C3	0.98368
C4	1.75743
C5	1.83215
Total	120.6338

and net molecular forces obtained at the MP2/cc-pvtz level for dimers. The interaction between dissimilar sites were determined by the popular Lorentz-Berthelotz combining rules as described in the Appendix. Hence, a total of 20 parameters were fitted. They are presented in the Table below for the model with explicit polarizability and the model without explicit molecular polarizability. To obtain the model which includes explicit polarizability, the

Table 4.7: *Ab Initio* Lennard-Jones Interaction Parameters

	Polarizable Model		Non-Polarizable Model	
Site Label	ϵ_{aa} [kcal/mol]	σ_{aa} [Å]	ϵ_{aa} [kcal/mol]	σ_{aa} [Å]
S	0.065263	3.720570	0.121480	3.61490
C1	0.006984	4.461090	0.000000	0.00000
C2	0.000000	0.000000	0.000000	0.00000
C3	1.266650	3.081990	0.095721	3.713780
C4	0.002685	4.824340	0.035175	4.086840
C5	0.002720	5.117790	0.246225	3.213820
H1	0.000000	0.000000	0.003109	2.878720
H2	0.000000	0.000000	0.001289	3.265710
H3	0.000000	0.000000	0.000000	0.000000
H4	0.000000	0.000000	0.007215	0.000000

forces arising from the molecular polarizability alone were first subtracted from the *ab initio* forces and the centre-of-mass torques and net molecular forces determined from the resulting forces. These were then fitted to obtain the LJ parameters shown in the Table above.

Observe that in both the polarizable and the non-polarizable models, the parameterization resulted in no LJ interaction between C2 and all the other atoms and also no LJ interaction between H3 and all atoms. Additionally, the polarizable model has no LJ interaction involving any hydrogen atom while the non-polarizable model has no LJ interaction between C1 and the other atoms.

Having obtained these parameters, the natural thing is to perform MD simulations which should be done in future work.

Bibliography

[1] Khanh Do, David M. Huang, Roland Faller, Adam J. Moule, Supplementary Information for: " A comparative MD study of the local structure of polymer semiconductors P3HT and PBTTT " *Department of Chemistry Engineering & Materials Science, University of California, Davis, CA 95616, USA*.

[2] W.L. Jorgensen, D.S. Maxwell, and J. Tirado-Rives, Supporting Information for:"Developing and Testing of the OPLS All Atoms Force Field on Conformational Energetics and Properties of Organic Liquids", *J. Am. Chem. Soc.* 118, 11225-11236 (1996).

[3] Cheung, D. L., McMahon, D. P. & Troisi, A., "Computational study of the structure and charge-transfer parameters in low-molecular-mass P3HT", *Journal of Physical Chemistry B 113*: 93939401, 2009b.

[4] T.H. Dunning, Jr. *J. Chem. Phys.* 90, 1007 (1989).

[5] M.C. Singh and P. A. Kollman, *J. Comp. Chem.* 5, 129-145 (1984).

Chapter 5

Conclusions and Recommendations

5.1 Conclusion

In this work, Poly (3-hexylthiophene) has been successfully modeled and we have shown that $(P3HT)_n$ (n = 1, 2 and 3) gets more polarizable with increasing monomer chains. A polarizable force field was developed that can be used for MD simulation.

From molecular dynamics simulations we have also found that the expansion of the alkyl side chain (C_nH_{2n+1}, $n = 6$) with temperature directly affects the molecular packing, which influences its morphology. The semi crystalline (less amorphous) behavior of $(P3HT)_n$ was confirmed between temperatures of 300 K and 400 K indicating the possible destruction of P3HT material at higher temperatures beyond 400 K during OPV fabrication process.

5.2 Recommendation

Since it is not clear that the linear trend observed in the variation of the number of P3HT units, **n** with polarizability would change, the need to optimize and perform MD simulations for higher **n** of $(P3HT)_n$ (i.e., for $n > 3$) in the future is recommended. There is also a need to perform MD simulations for $(P3HT)_1$ using the *ab initio* polarizable force field developed in this work.

Appendix

- **Born-Oppenheimer approximation**

  The Born-Oppenheimer Approximation is the assumption that the electronic motion and the nuclear motion in molecules can be separated which leads to a molecular wave function in terms of electron positions $\mathbf{r}_i$ and nuclear position, $\mathbf{R}_j$

  $$\Psi_{molecule}(\mathbf{r}_i, \mathbf{R}_j) = \Psi_{electrons}(\mathbf{r}_i, \mathbf{R}_j)\Psi_{nuclei}(\mathbf{R}_j) \tag{5.1}$$

  This involves the following assumptions:

  1. The electronic wavefunction depends on the nuclear positions but not on their velocities, i.e., the nuclear motion is so much slower than electron motion that they can be considered to be fixed.
  2. The nuclear motion (e.g., rotation, vibration) sees a smeared out potential from the speedy electrons

- **Proof of Hellmann-Feynman theorem**

  If we consider a system with a Hamiltonian, H(α) that depends on some parameters α. Where $|\psi(\alpha)\rangle$ is the eigen vector of H(α) with eigen value E(α), then the time independent Schrodinger equation is:

  $$H(\alpha)|\psi(\alpha)\rangle = E(\alpha)|\psi(\alpha)\rangle \tag{5.2}$$

  If it is further assumed that the eigen vector is normalized such that

  $$\langle\psi(\alpha)|\psi(\alpha)\rangle = 1 \tag{5.3}$$

the Hellmann-Feynman theorem states that

$$\frac{dE}{d\alpha} = \langle\psi(\alpha)|\frac{dH}{d\alpha}|\psi(\alpha)\rangle \tag{5.4}$$

Proof

Taking the inner product of equation(), we have

$$E(\alpha) = \langle\psi(\alpha)|H(\alpha)|\psi(\alpha)\rangle \tag{5.5}$$

Differentiating both sides with respect to α yields

$$\frac{dE}{d\alpha} = \langle\frac{d\psi(\alpha)}{d\alpha}|H(\alpha)|\psi(\alpha)\rangle + \langle\psi(\alpha)|\frac{dH}{d\alpha}|\psi(\alpha)\rangle + \langle\psi(\alpha)|H(\alpha)|\frac{d\psi(\alpha)}{d\alpha}\rangle \tag{5.6}$$

Since $|\psi(\alpha)\rangle$ is the eigen vector of H(α) with eigen value E(α), equation() can be written as

$$\begin{aligned}\frac{dE}{d\alpha} &= \langle\psi(\alpha)|\frac{dH}{d\alpha}|\psi(\alpha)\rangle + E(\alpha)\langle\frac{d\psi(\alpha)}{d\alpha}|\psi(\alpha)\rangle + E(\alpha)\langle\psi(\alpha)|\frac{d\psi(\alpha)}{d\alpha}\rangle \\ &= \langle\psi(\alpha)|\frac{dH}{d\alpha}|\psi(\alpha)\rangle + E(\alpha)\left[\langle\frac{d\psi(\alpha)}{d\alpha}|\psi(\alpha)\rangle + \langle\psi(\alpha)|\frac{d\psi(\alpha)}{d\alpha}\rangle\right]\end{aligned} \tag{5.7}$$

From the normalization condition:

$$\langle\psi(\alpha)|\psi(\alpha)\rangle = 1 \tag{5.8}$$

and

$$\langle\frac{d\psi(\alpha)}{d\alpha}|\psi(\alpha)\rangle + \langle\psi(\alpha)|\frac{d\psi(\alpha)}{d\alpha}\rangle = 0 \tag{5.9}$$

Hence the term in square brackets (Eq.) vanishes and we have

$$\frac{dE}{d\alpha} = \langle\psi(\alpha)|\frac{dH}{d\alpha}|\psi(\alpha)\rangle \tag{5.10}$$

which is the Hellman-Feynman theorem.

- **Length of MD simulation box calculation**

Density of P3HT (ρ) = 1.1 g/cm^3

Molecular mass of single unit P3HT (M)= 168.3005 $g/mol = 279.4695 \times 10^{-24}$ g.
$\therefore$ for n = 50 monomers, M = $50 \times 279.4695204 \times 10^{-24}$ g = $13973.47602 \times 10^{-24}$ g
Since

$$\rho = \frac{Mass}{Volume} = \frac{M}{V} \tag{5.11}$$

$$V = \frac{M}{\rho} = \frac{13973.47602 \times 10^{-30} g}{1.1 g/m^3} = 12703.16002 \times 10^{-30} m^3 \tag{5.12}$$

$\therefore$ the length of box (L) = $V^{1/3} = 23.327428$ $\mathring{A}$

- **Chosen combination rule for the Leonard- Jones parameters**

$$\sigma_{ij} = \frac{1}{2}(\sigma_{ii} + \sigma_{jj}) \tag{5.13}$$

$$\varepsilon_{ij} = (\varepsilon_{ii}\varepsilon_{jj})^{1/2} \tag{5.14}$$

- **Radial Distribution Function (RDF)**

This is an example of a pair correlation function which describes how on an average, the atoms in a system are radially packed around each other and it is denoted by g(r).
Mathematically,

$$g(r) = \frac{n(r)}{\rho 4\pi r^2 \Delta r} \tag{5.15}$$

where
r is the interatomic separation.
n(r) is the average number of atoms in a shell of width Δr at distance r.
ρ is the mean atomic density.